Carbon Energy

WILEY

CARBON ENERGY

REVIEW OPEN ACCESS

Advancements in Thermo and Photothermal CO_2 Hydrogenation to Light Olefins Using Fe-Based Catalysts: Current Progress and Future Directions

Timofey Karnaukhov | Blaž Likozar | Andrii Kostyniuk

Department of Catalysis and Chemical Reaction Engineering, National Institute of Chemistry, Ljubljana, Slovenia

Correspondence: Andrii Kostyniuk (andrii.kostyniuk@ki.si)

Received: 20 January 2025 | **Revised:** 24 March 2025 | **Accepted:** 5 April 2025

Funding: This study was supported by the Ministry of Higher Education, Science and Innovation, and the Slovenian Research Agency (ARIS) through research grants J7-4638 and J2-4441.

Keywords: CO_2 hydrogenation | heterogeneous catalysts | light olefins | photothermal catalysis | reaction mechanisms

ABSTRACT

The development of human industry inevitably leads to excessive carbon dioxide (CO_2) emissions. It can cause critical ecological consequences, primarily global warming and ocean acidification. In this regard, close attention is paid to the carbon capture, utilization, and storage concept. The key component of this concept is the catalytic conversion of CO_2 into valuable chemical compounds and fuels. Light olefins are one of the most industrially important chemicals, and their sustainable production via CO_2 hydrogenation could be a prospective way to reach carbon neutrality. Fe-based materials are widely recognized as effective thermocatalysts and photothermal catalysts for that process thanks to their low cost, high activity, and good stability. This review critically examines the most recent progress in the development and optimization of Fe-based catalysts for CO_2 hydrogenation into light olefins. Particular attention is paid to understanding the roles of catalyst composition, structural properties, and promoters in enhancing catalytic activity, selectivity, and stability.

1 | Introduction

In recent decades, the world community has become seriously concerned about the problems associated with climate change due to human activity. One of the most widely discussed problems is the increase of carbon dioxide (CO_2) concentrations in the Earth's atmosphere and ocean, leading to the greenhouse effect [1] and water acidification [2]. Being approximately constant over thousands of years during the preindustrial era, CO_2 levels are dramatically increasing nowadays [3].

In response to these challenges, the complex concept of carbon capture, utilization, and storage (CCUS) was proposed [4–9]. In particular, the capture technologies involve decreasing CO_2 emissions via post-combustion capture, precombustion capture, and oxy-fuel combustion ways [10]. In turn, the storage technologies imply CO_2 pumping into underground reservoirs, such as depleted oil and gas reservoirs or saline aquifers, for long-term containment [11]. Finally, the utilization technologies propose using CO_2 to produce valuable chemicals and fuels [12–14].

Therefore, the CCUS concept provides a new perspective on CO_2, considering it not only as a greenhouse gas but also as a cheap and renewable carbon source. A wide range of value-added products, such as chemicals, fuels, solid materials, and bio-products, can be generated starting from CO_2 (Figure 1) [15–17]. Among this variety of possible products, light olefins such as ethylene, propylene, and butylenes attract special attention. Being of the main industrial feedstocks for plastics, synthetic rubbers, solvents, surfactants, paintings, and other chemicals, light olefins are increasingly in

demand from year to year (Figure 2) [18]. This makes sustainable production of light olefins from CO_2 an attractive goal [19].

However, the high stability of CO_2 molecules is an essential natural hindrance to their conversion. For that reason, using special catalysts is an inevitable requirement for this process. Nowadays, several catalytic approaches are developed to address CO_2 activation issues, including homogeneous [20] and heterogeneous catalysis [21], and photo- [22], bio- [23], and electro-catalysis [24, 25]. Among these strategies, thermocatalytic activation over heterogeneous catalysts remains the most adjustable, scalable, and commercially prospective way of CO_2 conversion despite recent significant advances in other areas of catalysis [26].

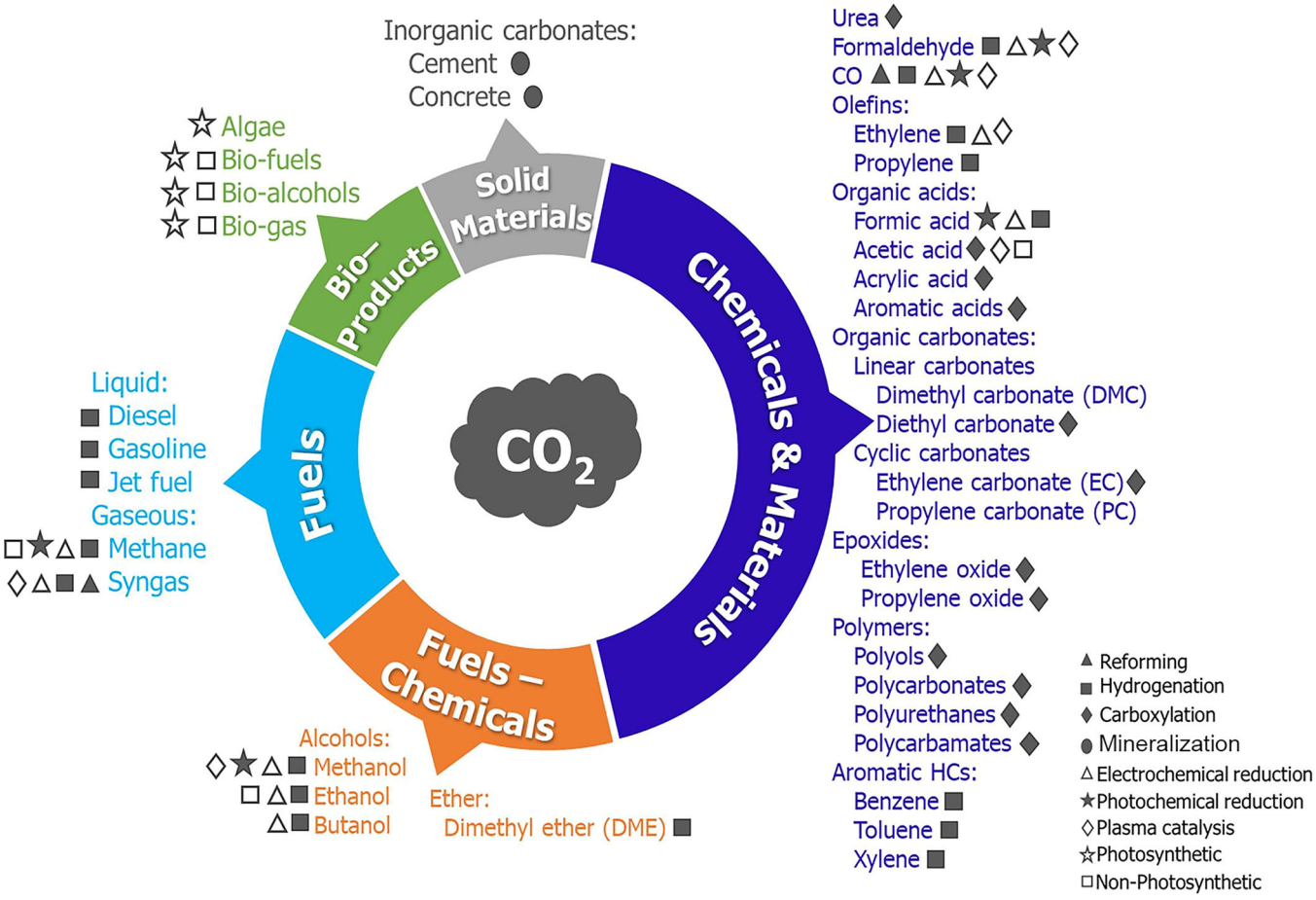

FIGURE 1 | Value-added products can be obtained using CO_2. Reproduced with permission: Copyright 2021, Elsevier [15].

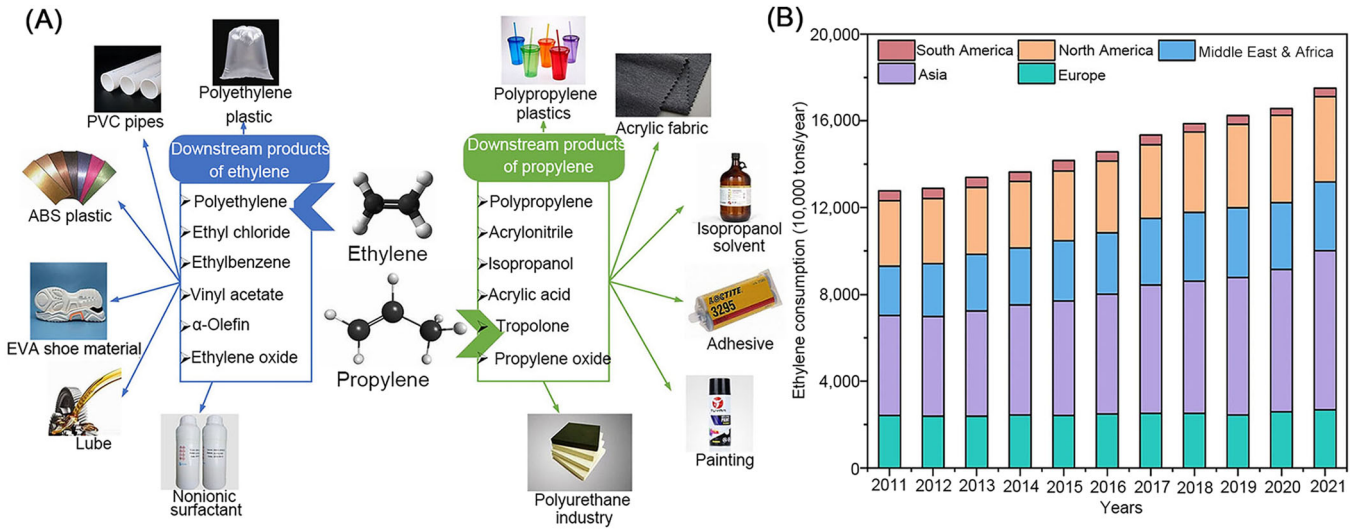

FIGURE 2 | (A) Light olefins as raw materials for value-added products. (B) World annual ethylene consumption. Reproduced with permission: Copyright 2024, John Wiley and Sons [18].

CO_2 hydrogenation stands out among thermocatalytic CO_2 conversion methods thanks to its lower energy requirements, reduced waste, potential for green hydrogen use, and scalability [27].

Iron (Fe)-based catalysts have emerged as one of the most promising candidates for facilitating CO_2 conversion into hydrocarbons. The abundance of Fe-based materials, their low cost, high catalytic activity, and good stability have driven significant research efforts in optimizing these catalysts for CO_2 hydrogenation. Moreover, tunable surface chemistry based on high sensitivity to promoters and supports provides wide possibilities for adjusting the selectivity of specific products [19, 28, 29]. All these advantages of Fe-based catalysts have attracted significant interest from the scientific community, expressed in many studies devoted to CO_2 hydrogenation into light olefins over these heterogeneous catalysts.

This review provides a comprehensive analysis of the current state of research on Fe-based catalysts for the thermocatalytic and photothermocatalytic hydrogenation of CO_2 into light olefins. We discuss key factors influencing catalyst performance, including the reaction conditions, alkaline and alkaline-earth promoters, the most studied Fe combinations with other transition metals (Zn, Mn, and Co), and the roles of the catalysts' supports. In addition, we analyze the mechanistic pathways of CO_2 hydrogenation, emphasizing the main opportunities to enhance the selectivity of light olefins. Finally, we address the future prospects of this technology, highlighting ongoing challenges and potential avenues for further catalyst optimization. Compared with previous reviews, this article provides a broader consideration of possible catalyst compositions and offers a more detailed analysis of the influence of promoters. Based on the most recent works (primarily from the last 5 years), this article provides the most up-to-date view of the state of the topic. Moreover, to our knowledge, this review describes and systematically analyzes for the first time the photothermal hydrogenation of CO_2 to light olefins over Fe-based catalysts.

2 | CO_2 Conversion: Thermodynamic Analysis

As outlined earlier, the CO_2 molecule is highly stable, making its transformation difficult. So, using CO_2 as the single reagent requires too much energy to be performed in moderate conditions (Table 1, Equation 1). At the same time, involving hydrogen as a reducing agent essentially facilitates CO_2 conversion (Table 1, Equation 2). In this regard, CO_2 conversion is mostly performed as CO_2 hydrogenation. Over Fe-based catalysts, it includes two main stages:

1. Reverse water gas shift (RWGS) reaction:

$$CO_2 + H_2 \leftrightarrow CO + H_2O$$

2. Fischer–Tropsch synthesis (FTS):

$$nCO + 2nH_2 \rightarrow C_nH_{2n} + nH_2O$$

$$nCO + (2n+1)H_2 \rightarrow C_nH_{2n+2} + nH_2O$$

In this regard, we propose to discuss the main thermodynamic parameters of the reactions under consideration and several principal side reactions (Table 1).

An analysis of the process trends reveals several important observations. The RWGS (Equation 2) is endothermic, requiring high operating temperatures to proceed effectively. In contrast, the reactions producing olefins from CO_2 (Equations 3–5) are exothermic, necessitating their operation at relatively lower temperatures. Additionally, within the homologous series, an increase in carbon atoms corresponds with a slight rise in average binding energy. This results in an enhanced thermal effect per CO_2 molecule, suggesting that lowering the reaction temperature may favor the formation of longer-chain products while reducing the selectivity toward light olefins. Moreover, similar exothermic behavior observed in the several side reactions (Equations 6 and 7 and analogous pathways) contributes to product formation under the same conditions, further diminishing the selectivity for light olefins at lower temperatures. Consequently, the reaction temperature should not be too low—not only due to kinetic limitations and reduced CO_2 conversion but also because of lower temperature increasing the fraction of C_{5+} products at the expense of light olefins selectivity. Conversely, excessively high temperatures favor the formation of C_1 products, particularly CO. Thus, the temperature of the reaction should be optimal. Most current studies have identified 320°C–340°C as the optimal range for light olefins production [30–39].

TABLE 1 | Standard enthalpies ($\Delta_r H°_{298}$) and Gibbs Free Energies ($\Delta_r G°_{298}$) for the reactions of CO_2 conversion into light olefins [21].

Equation number	Reaction	$\Delta_r H°_{298}$, kJ mol^{-1}	$\Delta_r G°_{298}$, kJ mol^{-1}
1	$CO_2 \rightarrow CO + \frac{1}{2}O_2$	293.0	257.2
2	$CO_2 + H_2 = CO + H_2O$	41.2	28.6
3	$CO_2 + 3H_2 \rightarrow \frac{1}{2}C_2H_4 + 2H_2O$	−64.0	−28.7
4	$CO_2 + 3H_2 \rightarrow \frac{1}{3}C_3H_6 + 2H_2O$	−83.6	−42.1
5	$CO_2 + 3H_2 \rightarrow \frac{1}{4}n-C_4H_8 + 2H_2O$	−90.3	−45.2
6	$CO_2 + 4H_2 = CH_4 + 2H_2O$	−165.0	−113.5
7	$CO_2 + 3H_2 = CH_3OH + H_2O$	−49.5	3.5

At the same time, all the reactions under discussion result in a decrease in the number of gas moles, except the RWGS reaction. This implies that increasing the reaction pressure should favor the conversion of CO_2 toward products that involve a reduction in gas moles, thereby decreasing the relative fraction of CO in the product mixture. Although several studies have examined light olefins production at atmospheric pressure, it must be acknowledged that CO remains the predominant product under such conditions even after catalyst optimization [40, 41]. While increasing the reaction pressure generally enhances the hydrocarbon fraction, excessive pressurization can promote the secondary hydrogenation of light olefins, leading to a higher yield of paraffinic products [30, 31, 35, 42]. Consequently, as with reaction temperature, an optimal pressure range exists. Although the optimal pressure may vary significantly from catalyst to catalyst, the highest selectivity for olefins is typically achieved at pressures between 2 and 3 MPa [30, 31, 35, 37–39, 42, 43].

The H_2/CO_2 ratio is another determinant of the CO_2 hydrogenation reaction. As can be seen from Table 1, the stoichiometric ratio for every olefin is 3, which is generally considered to be optimal [30, 31, 37, 39, 44]. Although increasing this ratio above the stoichiometric one enhances CO_2 conversion, it also promotes methanation and the secondary hydrogenation of olefins to paraffins [30, 31, 37, 39]. On the other hand, a decrease in the H_2/CO_2 ratio leads to higher CO selectivity to the detriment of the hydrocarbon fraction in general and light olefins in particular [31, 37, 39]. Also, the low H_2/CO_2 ratio can increase C_{5+} product selectivity [44].

Finally, contact time can be indicated as another important general parameter of the reacting system [45]. In the literature, it is usually represented as the gas hourly space velocity (GHSV). A low GHSV value (equivalent to high contact time) leads to high CO_2 conversion. However, in this case, light olefins selectivity decreases due to secondary olefins to paraffins hydrogenation and excessive chain growth producing C_{5+} products [30, 31, 34, 35, 38]. Thus, the highest yield of light olefins is achieved at optimal contact time, when high olefin selectivity is combined with appropriate CO_2 conversion.

3 | Alkali and Alkaline (Electronic) promoters of Fe-Based CO_2 Hydrogenation Catalysts

Although there are several publications on the activity of undoped Fe-based catalysts [46], it is widely accepted that significant improvements in results can be achieved by modifying these catalysts [47, 48]. In this section, we would like to discuss the doping of Fe-based catalysts with alkali and alkaline metals.

These promoters enhance the basicity of Fe-based catalysts, which as reported facilitate CO_2 adsorption and carbonization of Fe oxides [49]. Sodium (Na)-doped catalysts are characterized by a smaller particle size of the Fe_5C_2 phase and its more uniform distribution. Also, Na suppresses the hydrogenation of Fe_5C_2 and surface carbon, inhibiting alkanes formation [50, 51]. Moreover, it was shown that an increase in the Na content from 0.1 to 5 wt% leads to a consistent increase in the olefins/paraffins (O/P) ratio and selectivity of the C_2–C_7 olefins. However, increasing the Na content promotes hydrocarbon chain growth, which appears to reduce the proportion of C_2–C_4 olefins in the reported value for the 5%Na sample compared to the 3%Na sample [50]. Another example is the promotion of $CoFe_2O_4$ with Na [52]. Despite decreasing CO_2 conversion and enhanced C_{5+} product formation, the Na-promoted sample shows 6 times greater selectivity towards light olefins than the unpromoted one. The authors associated this effect with the facilitation of the active phase χ-Fe_5C_2 formation,

Potassium (K) has a similar effect on Fe-based catalysts. Thus, Zhu et al. [53] showed that K species enhances CO_2 adsorption on the Fe-based catalyst and facilitates CO formation on the RWGS step. Also, the presence of K species, as reported, accelerates the stepwise carburization of metallic Fe to Fe_3C and Fe_5C_2 at the beginning of the process. As a result, the K-promoted catalyst has a carbon-rich and oxygen-poor microenvironment on its surface, which prevents oxidation of the active Fe_5C_2 phase by water and CO_2. By varying the potassium content in the catalyst, 28.9% selectivity toward light olefins at 32.6% conversion of CO_2 was achieved. Russkikh et al. [54] managed to prepare an effective catalyst for CO_2 hydrogenation by promoting Fe-rich industrial waste (red mud) with K, which led to favoring CO_2 adsorption and hydrogenation of iron-containing species. After 50 h of reaction, K-promoted red mud provides 34% selectivity towards light olefins which is 2.6 times more than that for the unpromoted one with almost the same CO_2 conversion of 41%–42%. In one work [41], authors investigated K-promoted Fe-Ce-Zr catalysts for CO_2 hydrogenation at atmospheric pressure. Even though CO was the main product in these conditions in all cases, optimal K loading (2 wt%) increased olefins fraction in C_2–C_3 product up to > 90%. Further addition of K decreased light olefins selectivity, which was associated with an excessive increase in carbon concentration on the catalyst surface. It stabilized low-active carbide phases (primarily Fe_2C) and led to the layered carbon deposition with deactivation of the catalyst.

The effect of rubidium (Rb) on Fe-based catalysts for CO_2 hydrogenation was investigated by Sun et al. [55]. In this case, rising Rb content from 0 to 8 wt % increased the average chain length and the O/P ratio. Even the low Rb loading promoted light olefins formation, but methane and light paraffins selectivities remained high. At the same time, excessive Rb content led to increased selectivity of C_{5+} products. Thus, Rb can promote CO_2 adsorption and increase the surface C/H ratio, and this effect is enhanced with rising Rb content. Optimal results were reached over the 3wt%Rb/Fe_3O_4 catalyst (36.6% selectivity at 39.7% CO_2 conversion).

Zhou et al. conducted a systematic study on the effects of introducing alkali metals [56]. They prepared a series of Fe-Mo catalysts with different promoters (Figure 3). The study confirmed that adding any alkali metal increases the number of basic sites, thereby significantly enhancing the selectivity for light olefins. However, Na and K favor CO_2 conversion and the reaction rate while Rb and Cs decrease these values. The authors claimed that the electronegativity of the alkali promoter was a principal parameter of the catalytic ability of the Fe-Mo sample. Another systematic study of alkaline promoter effects was conducted by Barrios et al. [57]. Using ZrO_2-supported Fe_2O_3 modified by various metals (FeM/-ZrO_2), the authors confirmed that K addition facilitates CO_2

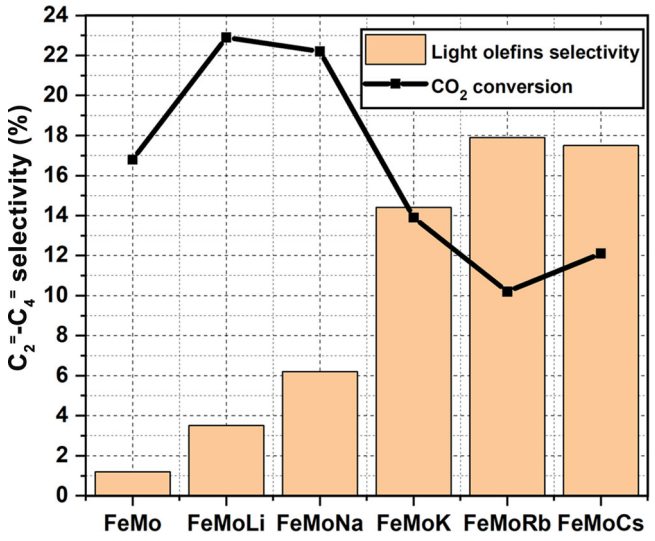

FIGURE 3 | Effect of alkali promoters on the FeMo catalyst for CO_2 hydrogenation into light olefins (based on the data from reference [56]).

adsorption and makes C–C coupling reactions preferable route compared with secondary hydrogenation processes (Figure 4A). However, K-promoted catalysts increase C_{5+} product fraction with CO_2 conversion, which is not observed for unpromoted ones (Figure 4B).

Combining alkali and alkaline metal promoters can provide additional enhancement in olefin production. Thus, moderate magnesium (Mg) addition in the KFeMn catalyst increases both CO_2 conversion and olefins selectivity [58]. It was stated that Mg can facilitate CO_2 adsorption while destabilizing adsorbed hydrogen species. Moreover, the Mg additive further accelerates the reduction and carburization of Fe oxide, which leads to the formation of the active carbide phases of FTS, promoting the conversion of the intermediate CO into hydrocarbons. Similarly, NaSrFe catalyst provides increased CO_2 conversion and value-added olefins selectivity [59]. Strontium (Sr) acts as a structural promoter, increasing the dispersion of iron-containing particles. In addition, the formation of the $SrCO_3$ phase facilitates the formation and stabilization of iron carbides, providing 500-h stable performance for the catalyst. Similar performance in the same conditions was observed for the NaBaFe catalyst [60], which was associated with a synergetic effect between Na and Ba. This effect accelerated lattice oxygen consumption, leading to an increased generation of oxygen defect sites and enhanced CO_2 activation. Furthermore, the formation of active iron carbide was promoted, and its stability was maintained throughout the reaction. In the study [61], a series of $Ca_{2-x}K_xFe_2O_5$ materials (where $x = 0–1.2$) was prepared. In this case, Ca-containing samples had many strong basic sites and oxygen vacancies (OV). In turn, the K promoter further enhances surface basicity and, more importantly, improves catalyst dispersity while facilitating C-O dissociation and C-C coupling. The best CO_2 conversion, light olefin selectivity, and O/P ratio were obtained over the $Ca_{1.0}K_{1.0}Fe_2O_5$ catalyst. Chen et al. [62] developed a mechanochemical technique to incorporate Mg into the iron oxide structure. In addition to the basic effects of electronic promoters, resulting "O-Fe/Mg-O" species promote both CO_2 adsorption and RWGS reaction via *COOMg intermediates formation. Therefore, $Fe_3O_4/Mg/K_2CO_3$ reached 46.4% of light olefin selectivity at 32.1% CO_2 conversion. Table 2 summarizes the catalytic performance of electronically promoted Fe-based catalysts and compares them to unpromoted ones.

4 | Two-Component Fe-Containing Catalysts

Fe-based catalysts can be further optimized by incorporating other transition metals. Such combinations can improve catalyst performance and enhance selectivity towards light olefins by forming joint phases or active interfaces. In this section, we would like to consider the most studied combinations and propose a detailed analysis of the corresponding studies.

4.1 | Fe-Zn Catalysts

Many current works confirm that the Zn addition to Fe-based catalysts favors the Fe_5C_2 phase formation and stabilization during CO_2 hydrogenation [43, 51, 63–65]. In particular, it was reported that Zn promoted the reduction and carburization of iron catalysts [63, 65] as well as prevented the reoxidation of iron carbides and carbon deposition on the catalyst surface [64]. Moreover, the addition of Zn in the amount of $ZnFe_2O_4$ spinel stoichiometry has been reported to increase surface basicity and promote CO_2 adsorption [66].

However, there are some controversial reports on the effects of Zn insertion. For instance, work [65] indicates that adding Zn to a pyrolytically prepared Fe/C catalyst enhances the secondary hydrogenation of the produced light olefins. At the same time, zinc oxide reduces the secondary hydrogenation of olefins on a co-precipitated Fe-Na catalyst [63]. In the study [67], the influence of the preparation method of Fe-Zn-K catalysts on its performance was consistently studied. The S-2Fe-1Zn-K sample, prepared via a solvothermal method, exhibits the highest surface basicity and provides the highest O/P ratio of 6.84. At the same time, it produces the largest amount of CO. The highest selectivity for light olefins (54.18%) was obtained using a co-precipitated C-2Fe-1Zn-K catalyst. Among the 2Fe-1Zn-K samples, hydrothermal H-2Fe-1Zn-K catalyst showed the smallest light olefins selectivity and O/P ratio. The authors attribute the olefins' productivity to the strong interaction between Zn and Fe species, while the separate ZnO phase decreases the selectivity of light olefins. The work [68] draws similar conclusions that ZnO promotes CH_4 and CO generation. However, it is also noted that excessive formation of the $ZnFe_2O_4$ phase can hinder catalyst activation. In this case, the best light olefins selectivity was obtained for 1Fe-1Zn-K catalyst (33.9% while CO_2 conversion was 54.0%). On the other hand, several studies note increasing both CO_2 conversion and light olefins selectivity over ZnO-χ-Fe_5C_2 interface [43, 63]. So, the study [43] proposes a presumable mechanism of CO_2 hydrogenation over ZnO-χ-Fe_5C_2 dual sites (Figure 5).

In the proposed scheme (Figure 5), ZnO catalyzes the RWGS reaction, while χ-Fe_5C_2 is responsible for Fischer–Tropsch olefin synthesis. Initially, CO_2 and H_2 are adsorbed onto the zinc oxide surface, where a hydrogenation reaction occurs between

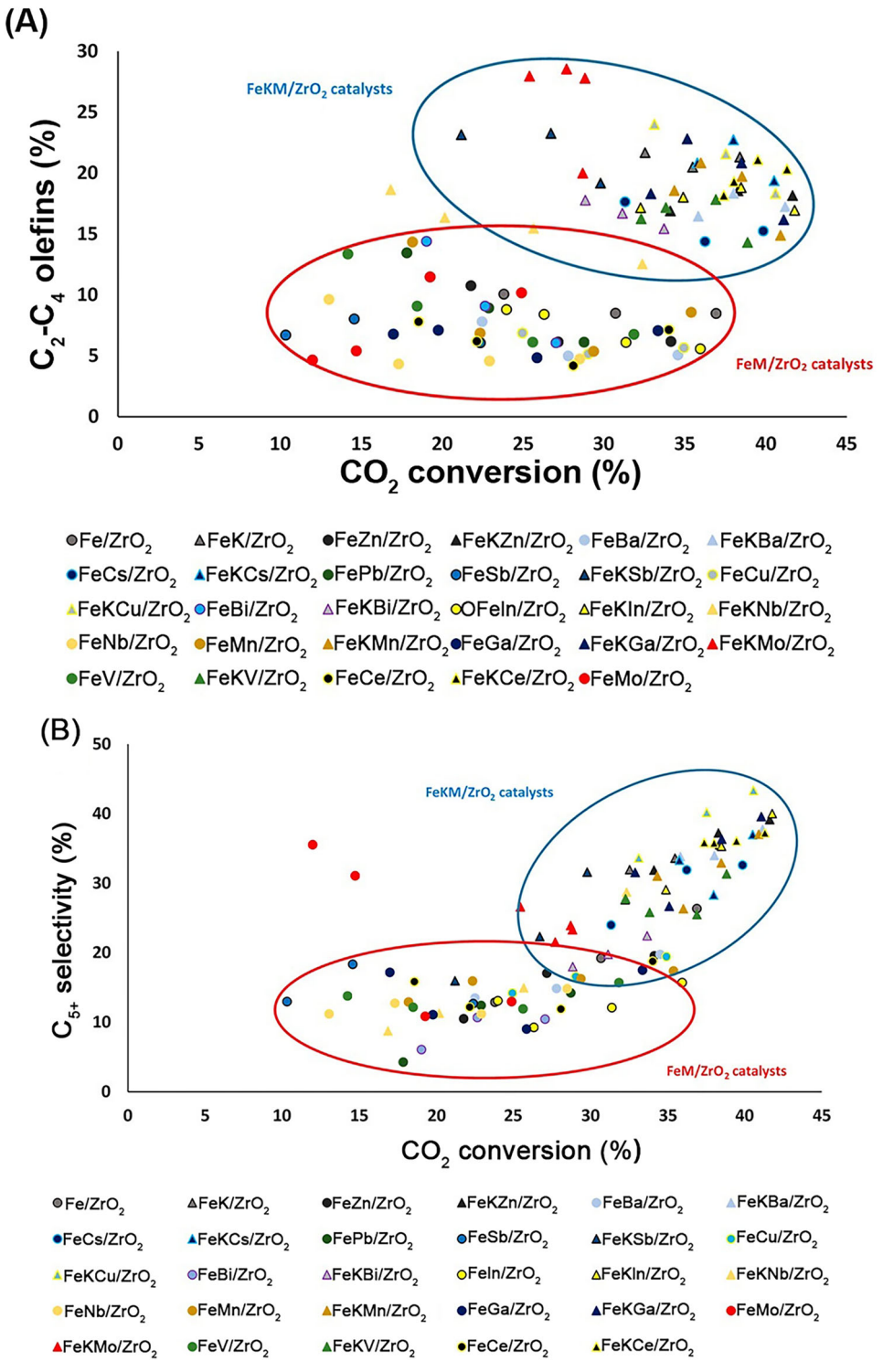

FIGURE 4 | (A) Light olefin selectivity and (B) C_{5+} selectivity vs. CO_2 conversion over Fe/ZrO_2 catalysts. $T = 350°C$, $P = 10$ bar, WHSV = 4.67–18.19 L g^{-1} h^{-1}, $H_2/CO_2 = 3$, time-on-stream (TOS) = 50 h. Reproduced with permission: Copyright 2022, American Chemical Society [57].

the adsorbed CO_2* and H* species forming CO* and OH*. The OH* species subsequently reacts with H*, transforming into water and not participating further in the main reaction mechanism. In contrast, the CO* species can diffuse onto the surface of iron carbide, where it undergoes further hydrogenation to produce olefins. This mechanism highlights the potential for other metal oxide phases to act as active components in the RWGS reaction instead of iron oxide, achieving up to 36% selectivity for light olefins.

Li et al. [69] confirmed that the Zn addition noticeably improved the stability of Fe-Na catalysts that facilitated producing light olefins during 1000 h without essential deactivation of catalyst 1.5Na-Fe-Zn, which was explained with the optimal

TABLE 2 | Alkali and alkaline promoting of Fe-based CO_2 hydrogenation catalysts into light olefins.

Catalyst	CO_2 conv. (%)	Product selectivity (%)					light olefin yield (%)	O/P	Reaction conditions			Ref.
		CO	CH_4	C_2^0-C_4^0	$C_2^=$-$C_4^=$	C_{5+}			GHSV, (mL g^{-1} h^{-1})	*T* (°C)	*P* (MPa)	
$Ca_{1.0}K_{1.0}Fe_2O_5$	46.33	40.43	15.35	4.16	34.59	5.47	16.03	8.31	7200	340	1.50	[61]
Na-$CoFe_2O_4$	41.8	9.7	20.0	6.9	37.2	26.2	15.5	5.4	7200	320	3.0	[52]
$CoFe_2O_4$	56.7	2.6	32.1	41.8	6.2	17.3	3.5	0.1				
Fe_3O_4/Mg/K_2CO_3	32.1	16.3	N/A	N/A	46.4	N/A	14.9	N/A	9600	320	1.0	[62]
3 wt%Rb/Fe_3O_4	39.7	8.1	15.1	3.4	36.6	22.2	14.5	10.7	2500	300	0.5	[55]
Red Mud + 2 wt% of K	41	26	19	6	34	15	14	6	9600	375	3	[54]
Red Mud	42	17	43	21	13	6	5	0.6				
0.5K-Fe	32.6	24.8	10.8	5.1	28.9	30.4	9.4	5.6	N/A	320	3.0	[53]
NaSrFe	40.5	8.3	8.9	N/A	71.1 ($C_{2+}^=$)	58.0 ($C_{4+}^=$)	28.8*	N/A	8000	320	3.0	[59]
NaBaFe-0.5	39.6	8.4	8.9	N/A	71.4 ($C_{2+}^=$)	58.2 ($C_{4+}^=$)	28.3*	N/A				
NaFe	37.1	10.2	9.5	N/A	66.9 ($C_{2+}^=$)	54.5 ($C_{4+}^=$)	24.8*	N/A				[60]
5%Na	34.67	12.37	22.80	0.2 (C_2^0-C_7^0)	54.37 ($C_2^=$-$C_7^=$)	1.49 ($C_{8+}^=$)	18.85**	6.06**	10,000	290	1.50	[50]
3%Na	32.54	15.69	24.34	8.49 (C_2^0-C_7^0)	52.58 ($C_2^=$-$C_7^=$)	1.26 ($C_{8+}^=$)	17.11**	6.19**				
0%Na	31.40	8.53	42.01	28.69 (C_2^0-C_7^0)	20.20 ($C_2^=$-$C_7^=$)	0.52 ($C_{8+}^=$)	6.34**	0.70**				
$KFeMnMg_{0.15}$	25.2	19.6	20.3	10.9 (C_{2+}^0)	49.2 ($C_{2+}^=$)		12.4*	4.5*	4000	320	3.0	[58]
KFeMn	20.4	27.6	15.3	11.9 (C_{2+}^0)	45.1 ($C_{2+}^=$)		9.2*	3.8*				
FCZ-K2	29.0	95.0	1.7	8.96 (C_2^0-C_3^0)	2.7 ($C_2^=$-$C_3^=$)	N/A	0.8***	15.9***	3200	370	0.1	[41]
FCZ	26.6	78.0	13.9	6.4 (C_2^0-C_3^0)	2.0 ($C_2^=$-$C_3^=$)	N/A	0.5***	0.3***				

*C_{2+} olefins yield and O/P ratio for C_{2+} hydrocarbon products.
**C_2–C_7 olefins yield and O/P ratio for C_2–C_7 hydrocarbon products.
***C_2–C_3 olefins yield and O/P ratio for C_2–C_3 hydrocarbon products.

iron-containing phase distribution. Moreover, light olefins selectivity was further improved up to the excellent 64.6% via catalytic cracking of C_{5+} products over ZSM-5 nanosheets. Table 3 summarizes the reported results for Fe-Zn binary catalysts for CO_2 hydrogenation into light olefins.

4.2 | Fe-Mn Catalysts

Manganese (Mn) is another widely used modifier for Fe-based catalysts in CO_2 hydrogenation. However, its application has yielded both positive and negative results, possibly due to variations in the interaction strength between Fe and Mn.

For example, Zhang et al. [70] examined a row of the 1%Na-Fe catalysts doped with different Mn amounts. They showed that the very addition of manganese, and a consistent increase in its content, reduces both CO_2 conversion and selectivity towards light olefins while selectivity towards CO increases. Contrary, study [71] demonstrated that an optimum in Mn content can be found: catalysts with (0.05–0.1)/1 of the Mn/Fe molar ratio showed about 63% C_2-C_5 products selectivity, but the O/P ratio was less than 1. Yang et al. [63] showed that Mn can strongly interact with Fe inhibiting the formation of iron carbides. This

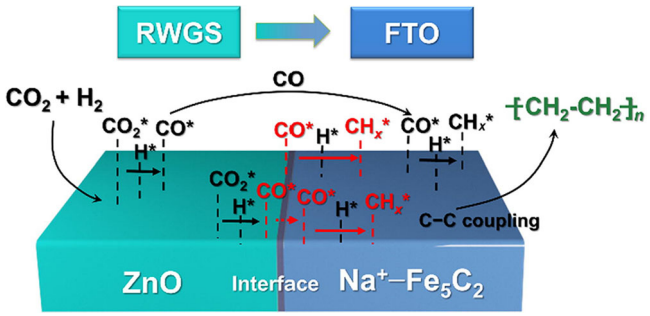

FIGURE 5 | Plausible CO_2 hydrogenation mechanism over the ZnO-χ-Fe_5C_2 interface. Reproduced with permission: Copyright 2021, Elsevier [43].

led to weak binding of CO and its high proportion in the mixture of products instead of the target ones.

At the same time, it was shown that Mn (as well as Zn) promotes the carburization of the pyrolytic-prepared Fe/C catalyst intensifying Fe_5C_2 active phase formation. Moreover, manganese inhibits the secondary hydrogenation of light olefins while Zn promotes it [65]. In study [45], Mn addition to the Fe_3O_4 microspheres enhances light olefins yield via both CO_2 activation and inhibiting of secondary hydrogenation of the olefins. Singh et al. [31] demonstrated that Mn doping of the Na-$CuFeO_2$ sample increases the number of weak basic sites and promotes reducibility and carburization of the catalyst. The density functional theory (DFT) calculation indicated a decrease in the activation energy barrier for generating OV in this case. The work [72] points to a similar effect. In addition, it highlights the synergy between Na and Mn promoters, preventing excess carbon chain growth and promoting the β-H abstraction of the short alkyl-metal intermediates, leading to the formation of light olefins. In turn, Xu et al. [73] found that close Fe–Mn contact could negatively affect both the intrinsic RWGS reaction rates and the olefin selectivity in CO_2 hydrogenation due to the Mn-promoted transformation from the RWGS-active iron oxide phase to the FTS-active Fe_5C_2 phase. Additionally, the steric hindrance of the Mn moiety to the FTS steps on the Fe_5C_2 sites suppressed the formation of olefins. Nevertheless, simultaneous modification of the iron catalyst with Na and Mn transforms the Mn into an effective promoter via weakening the initially strong Fe-Mn interaction. As a result, a high O/P ratio = 8.1 was achieved for the co-precipitated FeMnNa catalyst. Table 4 summarizes performance values for the Fe-Mn catalysts under discussion.

4.3 | Fe-Co Catalysts

Several studies report that adding cobalt improves the performance of Fe-based catalysts. Generally, the close proximity of Fe and Co in bimetallic catalysts is considered a key factor in

TABLE 3 | Fe-Zn catalysts for CO_2 hydrogenation into light olefins.

Catalyst	CO_2 conv. (%)	Product selectivity (%)					light olefin yield (%)	O/P	Reaction conditions			Ref.
		CO	CH_4	C_2^0-C_4^0	$C_2^=$-$C_4^=$	C_{5+}			GHSV, (mL g^{-1} h^{-1})	*T* (°C)	*P* (MPa)	
C-2Fe-1Zn/K	54.76	4.58	21.80	8.06	54.18	10.38	29.67	6.72	1000 h^{-1}	320	2.00	[67]
H-2Fe-1Zn/K	51.66	7.76	20.12	7.65	49.98	12.47	25.82	6.54				
S-2Fe-1Zn/K	46.34	10.01	21.38	7.33	50.08	10.14	23.21	6.84				
1Fe-1Zn-K	54.00	6.29	26.29	4.36	33.87	12.17	18.29	7.78	1000 h^{-1}	320	0.50	[68]
Na-Zn-Fe	38	15	11	4.2	36	34	14	8.5	15,000	340	2.5	[43]
FeZn-Na	37.5	11.5	13.3	6.0	32.7	36.6	12.3	5.5	4000	320	3.0	[63]
1.5Na-Fe1Zn1	39.0	15.6	10.7	3.6	29.1	40.9	11.3	8.0	1200	320	1.0	[69]
Fe-Zn	26.3	34.9	17.5	3.4	32.0	12.2	8.4	9.5	17,910	330	1.5	[64]
$ZnFe_2O_x$	34.6	17.1	22.3	19.2	24.4	16.9	8.4	1.3	2400	300	1.0	[66]
ZnFe/C	40.60	22.91	20.57	9.56	15.73	31.24	6.39	1.65	12,000	400	2.0	[65]
Fe-Zn-2Na	43	15.7	22.8	7.4 (C_2^0-C_6^0)	54.1 ($C_2^=$-$C_6^=$)		23.3*	7.3*	10,000	320	1.5	[51]

*C_2–C_6 olefins yield and O/P ratio for C_2–C_6 hydrocarbon products.

TABLE 4 | Fe-Mn catalysts for CO_2 hydrogenation into light olefins.

Catalyst	CO_2 conv. (%)	Product selectivity (%)					light olefin yield (%)	O/P	Reaction conditions			Ref.
		CO	CH_4	C_2^0-C_4^0	$C_2^=$-$C_4^=$	C_{5+}			GHSV, (mL g^{-1} h^{-1})	*T* (°C)	*P* (MPa)	
10Mn-Fe_3O_4	44.7	9.4	20.0	6.4	41.8	22.4	18.7	6.5	4000	350	2.0	[45]
2.5Mn/NCFO	36.6	33.5	13.1	9.4	35.7	8.5	13.1	3.8	3600	320	2.0	[31]
0.19Mn/ Fe_3O_4-NaAc	27.0	25.2	10.5	5.8	30.1	28.3	8.1	5.2	40 g h mol^{-1}	320	0.5	[72]
Fe_3O_4-NaAc	30.4	18.5	9.8	3.7	23.9	44.2	7.3	6.5				
MnFe/C	37.60	28.29	12.03	5.38	12.79	41.51	4.81	2.38	12,000	400	2.0	[65]
FeMnNa	35.0	18.1	10.7	31.7 (C_2–C_4)		39.5	22.2*	8.1*	12,000	340	2.0	[73]

*C_{2+} olefins yield and O/P ratio for C_{2+} hydrocarbon products.

promoting the preferential formation of light olefins. At the same time, separate Co sites yield CH_4 as a main product [52, 74, 75]. So, study [76] suggests a reactive ball milling technique to prepare Fe-Co bimetallic catalysts. Mechanical activation facilitates joint phase formation leading to CO_2 activation and accelerated C-C coupling. As a result, 50.4% of light olefin selectivity was achieved at 31.4% of CO_2 conversion. In the work [74], the Co/Fe ratio was varied from 0.25 to 4 in bimetallic catalysts. As a result, the best light olefins selectivity was achieved for the Co1Fe2 catalyst. In this case, joint χ-$(Co_xFe_{1-x})_5C_2$ active phase formation was observed. Further addition of cobalt led to the Co_2C phase formation, which was inactive for light olefins production. Moreover, the co-precipitated catalyst demonstrated a much higher space-time yield (STY) of olefins than the impregnated one, a result attributed to the closer proximity of the active metals (Figure 6).

Xu et al. [75] reported that Co incorporation to $ZnFe_2O_4$ spinel decreases both χ-Fe_5C_2 content and the average chain length. Also, θ-Fe_3C phase forming in this case, might inhibit secondary hydrogenation of the olefins producing. A series of core-shell Na/Fe@Co bimetallic structures were prepared by Li et al. [77]. These catalysts are reported to possess both enhanced reducibility and carburization ability as well as suitable surface basicity. As a result, the optimal Na/Fe@CoCo-3 catalyst showed an improved light olefin selectivity of 33.8% and a high O/P ratio of 7.5 at CO_2 conversion of 50.3% while CO selectivity was only 4.6%. The study [78] concentrates on the role of Co addition in the long-term stabilization of the Fe/K-Al_2O_3 catalyst. In the absence of cobalt, this catalyst deactivated noticeably through carbon deposition, sintering, and the active iron carbide phases reoxidation. An increase in the hydrogen fraction in the reagent's mixture decreased carbon fibers and wax deposition but destabilized the iron carbide phases. At the same time, Co additive promoted hydrogen spillover, thereby preventing catalyst carbonization. Moreover, cobalt incorporation enhanced the iron carbide species stability, inhibiting their transformation into oxides. The sintering resistance of the catalyst was also improved in the presence of cobalt.

Finally, many studies have reported on Fe-Co bimetallic catalysts supported on various materials, including oxides, carbon, zeolites, and others. Such catalysts will be discussed later in the corresponding chapters. Table 5 summarizes the Fe-Co catalysts performance data.

As an interim conclusion, we propose a graphical comparison of the most competitive two-component Fe-containing catalysts (Figure 7). The figure indicates that no single modifier demonstrates inherent superiority, as high CO_2 conversion rates and light olefins selectivity can be achieved with Fe-Zn, Fe-Mn, and Fe-Co catalysts alike. At the same time, improved catalytic performance is observed when special attention is paid to the synthesis method and the development of the catalyst structure.

5 | Supported Fe-Based Catalysts

Different supporting materials are widely used to improve heterogeneous catalysts. They can provide developed structure, dispersion, and stability of an active component as well as enhanced mechanical strength of a catalyst. Support can also serve as a co-catalytic phase, modifying the acid–base and electronic properties of a catalyst surface, facilitating adsorption-desorption processes, and inhibiting catalyst poisoning.

Moreover, in the case of Fe-based catalysts, support can regulate phase composition forming during the reaction, thus determining product distribution. So, Liu et al. [79] compared ZrO_2, carbon nanotubes (CNT), Al_2O_3, and SiO_2 as supports for Fe-based catalysts. It was shown that surface carbonization is increasing in the sequence: $SiO_2 < Al_2O_3 <$ CNT $< ZrO_2$. Orderliness of surface carbon species also rises in this sequence: Fe_5C_2 phase percentage varies from 19.2% in the FeNa/SiO_2 sample to 89.4% in the FeNa/ZrO_2 one. Moreover, it correlates with C_2–C_7 olefins selectivity: the best 54.1% value and O/P = 8.05 were obtained for the FeNa/ZrO_2 catalyst while the FeNa/SiO_2 predominantly produces CO. The authors associated this effect with increasing carbon oxides adsorption of the catalyst's surface with a simultaneous decrease in H_2 adsorption intensity, which increases the C/H surface ratio.

Bao et al. [80] synthesized iron catalysts over several metal oxide supports (TiO_2, Al_2O_3, ZrO_2, and CeO_2). They showed that iron-support interactions in the precursors gradually strengthened in the following order of supports: $TiO_2 < Al_2O_3 \approx ZrO_2 < CeO_2$. Weak interaction between Fe and TiO_2 results in predominant FeO_x species formation while strong Fe-CeO_2 interaction primarily forms Fe_5C_2 species. In turn, moderate iron-support interaction causes the presence of both

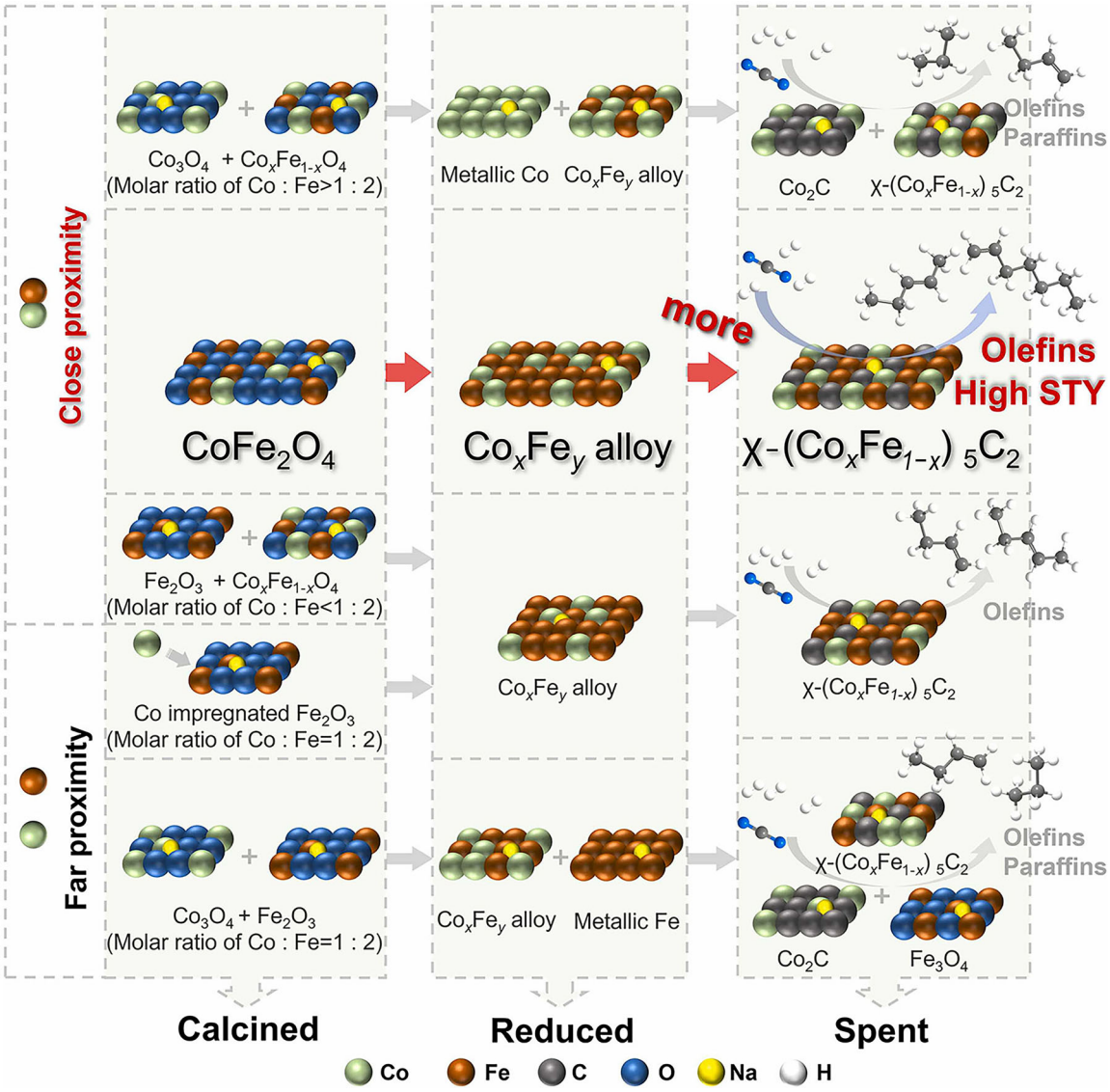

FIGURE 6 | Structural evolution of the Fe-Co catalysts and their performance. Reproduced with permission: Copyright 2023, Elsevier [74].

key phases in the Fe/Al_2O_3 and Fe/ZrO_2 catalysts. So, surface oxide and carbide phases demonstrate synergy in these cases, activating the H_2 and CO intermediate. For that reason, Fe/Al_2O_3 and Fe/ZrO_2 catalysts demonstrate essentially better light olefins selectivity than Fe/TiO_2 and Fe/CeO_2 ones (Table 6).

Dolsiririttigul et al. [81] systematically investigated iron-support interactions in FeCo/K catalysts of syngas conversion into light olefins. In their study, the support effect was primarily manifested in the dispersion of iron species and its influence on the Fe_5C_2 active phase formation. So, the FeCo/KSi catalyst contained small iron particles isolated within the SiO_2 support matrix. It hindered the active iron carbide phase generation and resulted in lower light olefins production. In turn, TiO_2 strongly interacted with iron oxide species, hampering their reduction and carburization. Finally, the Al_2O_3 support moderately interacted with iron species, providing a higher dispersion of the catalyst components and facilitating the Fe_5C_2 phase formation, which enhanced light olefins production.

In the following subsections, we provide a more detailed discussion of recent studies devoted to Fe-catalysts on different supports for light olefins production via CO_2 conversion.

5.1 | Al_2O_3-Supported Fe-Based Catalysts

Aluminum oxide is extensively studied support for Fe-based catalysts for CO_2 conversion into value-added products owing to its high surface area, superior mechanical properties, and adjustable pore size [82–84].

Chaipraditgul et al. [85] examined the influence of adding transition metals (Cu, Zn, Co, Mn, and V) to $Fe/K\text{-}Al_2O_3$ catalysts (Figure 8A). They showed that incorporating either Cu or Zn into the Fe-K catalyst enhances CO_2 conversion and reduces CH_4 formation, but it also leads to more C_{5+} products. In this case, Cu and Zn promote weakly adsorbed CO* species formation during the RWGS reaction. These species readily insert into adsorbed C_xH_y fragments, enhancing the formation of

TABLE 5 | Fe-Co catalysts for CO_2 hydrogenation into light olefins.

Catalyst	Product selectivity (%)					light olefin yield (%)	Reaction conditions			Ref.
	CO_2 conv. (%)	CO	CH_4	C_2^0-C_4^0	$C_2^=$-$C_4^=$	C_{5+}		O/P	GHSV, (mL g^{-1} h^{-1})	*T* (°C)	*P* (MPa)	
Na/Fe@CoCo-3	50.3	4.6	12.9	4.5	33.8	41.5	17.0	7.5	5 g h mol^{-1}	330	3.0	[77]
Co-Fe bimetallic	31.4	12.1	N/A	N/A	50.4	19.6	15.8	N/A	9600	320	1.0	[76]
Na-$CoFe_2O_4$	41.8	9.7	20.0	6.9	37.2	26.2	15.5	5.4	7200	320	3.0	[52]
2 wt%K-$ZnCo_{0.5}Fe_{1.5}O_4$	39.1	13.6	15.3	4.9	31.9	34.3	12.5	6.5	24,000	320	2.5	[75]
Co1Fe2	40.9	9.5	9.2	38.5 (C_2–C_4, O + P)	60.6 ($C_{2+}^=$)	35.9 ($C_{5+}^=$)	24.8*	N/A	8000	340	2.0	[74]

*C_{2+} olefins yield.

longer-chain hydrocarbon. In contrast, the Mn-promoted Fe-K catalyst significantly increased the olefin-to-paraffin ratio but decreased CO_2 conversion. In its turn, Cu, Co, and Zn essentially increase the amount of weakly adsorbed hydrogen atoms, promoting secondary hydrogenation of the formed olefin. Nevertheless, the Fe-Co/K-Al_2O_3 catalyst provides the highest light olefins selectivity of 40.5%, as Co could accelerate both the RWGS and CO hydrogenation reactions.

Numpilai et al. [83] compared the performance of the Fe-Co/K-Al_2O_3 catalysts, pre-calcined at different temperatures from 400°C to 800°C. They demonstrated that increasing temperature leads to particle size growth and decreasing reducibility of iron oxide. However, the F-700 sample exhibited the best O/P ratio = 7.6 which can be explained by $KAlO_2$ joint phase formation effectively preventing secondary hydrogenation. At the same time, the F-600 sample provided the best light olefins selectivity. Another study [84] was devoted to determining the most appropriate Al_2O_3 pore size (Figure 8B). It was shown that increasing support pore size led to the growth of iron crystallites and facilitated their reduction. In turn, it enhances the activity of the catalyst and selectivity towards hydrocarbons, including light olefins. Large catalyst pore size also facilitates product diffusion and increases the O/P ratio. However, increasing the catalyst pore size led to a higher selectivity for C_{5+} products, which reduced the selectivity for light olefins. So, the large-pore CL-Al_2O_3 sample (152.3 nm) exhibited lower light olefins selectivity than the medium-pore CM-Al_2O_3 sample (49.7 nm).

Witoon et al. [86] showed that the preparation method of Fe-Co/K-Al_2O_3 catalysts significantly affects their phase composition, reducibility, adsorption-desorption properties, and overall catalytic performance. They demonstrated that, among the catalysts prepared, the one-pot C1 sample achieved the highest CO_2 conversion and hydrocarbon selectivity, attributed to its superior Brunauer-Emmett-Teller (BET) surface area and well-developed small-mesoporous structure. However, potassium was not precipitated with the other metal oxides by this method, which made paraffins the main fraction in the product distribution. In turn, the stepwise precipitation-reduction prepared catalyst C3 enhanced the reducibility of metal oxides, providing many medium CO_2 adsorption sites and decreasing the number of weak H_2 adsorption sites. This catalyst showed the best selectivity towards light olefins (39.3%) among those studied. Polsomboon et al. [87] proposed a microwave calcination technique to prepare Fe-Co/K-Al_2O_3 catalysts. In this case, an increase in the microwave power from 364 to 700 W enhanced the Fe-K interactions, thereby raising the O/P ratio. At the same time, the best light olefins yield of 24.5% was achieved at the medium-high 616 W power level because of the optimal FeC_x/Fe_3O_4 ratio of 0.34.

In the work [36], a different amount of Zn (0–1.74 wt%) was added to the Fe-Co/K-Al_2O_3 composition. It was shown that Zn addition enhanced the dispersion of iron species and facilitated their reducibility, thus forming more adsorption sites. At the same time, Zn loading to the Fe-Co/K-Al_2O_3 catalyst promoted hydrogen adsorption and decreased the O/P ratio. The best yield of light olefins (19.9%) at the selectivity optimum (37%) was achieved for the 0.58%Zn-Fe-Co/K-Al_2O_3 catalyst. Dai et al. [44] modified the Fe-Co/Al_2O_3 catalyst with EDTA-2Na. It was

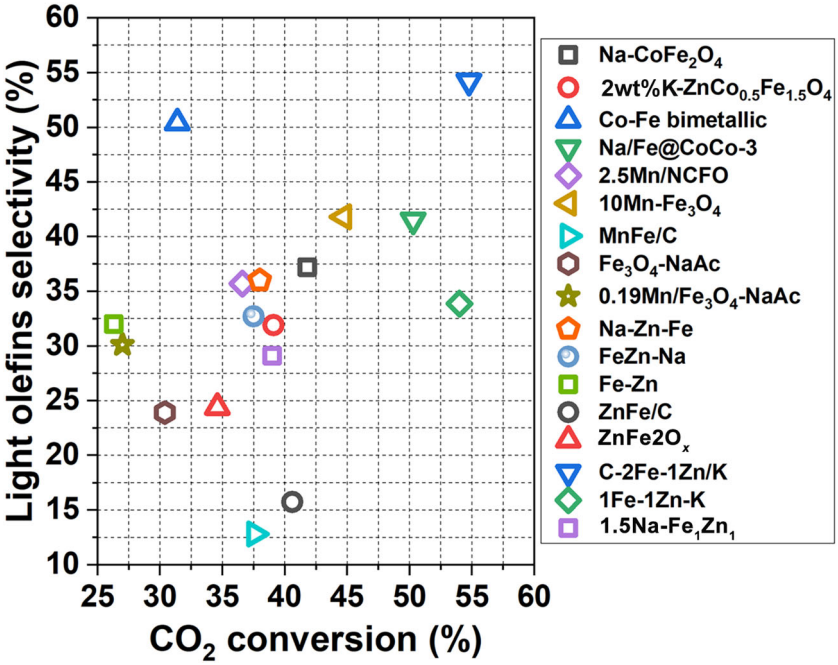

FIGURE 7 | Performance comparison of two-component Fe-based catalysts.

TABLE 6 | Supported Fe-based catalysts for CO_2 hydrogenation: Supports comparison.

Catalyst	CO_2 conv. (%)	Product selectivity (%)					light olefin yield (%)	O/P	Reaction conditions			Ref.
		CO	CH_4	C_2^0-C_4^0	$C_2^=$-$C_4^=$	C_{5+}			*GHSV* (ml g^{-1} h^{-1})	*T* (°C)	*P* (MPa)	
FeNa/ZrO_2	32.7	17.1	22.1	6.7 (C_2^0-C_7^0)	54.1 ($C_2^=$-$C_7^=$)		17.7*	8.1*	9000	320	2.0	[79]
FeNa/CNT	31.5	16.5	23.3	11.7 (C_2^0-C_7^0)	48.5 ($C_2^=$-$C_7^=$)		15.3*	4.1*				
FeNa/Al_2O_3	38.5	10.0	35.6	27.3 (C_2^0-C_7^0)	27.2 ($C_2^=$-$C_7^=$)		10.5*	1.0*				
FeNa/SiO_2	18.9	68.4	22.1	2.7 (C_2^0-C_7^0)	2.7 ($C_2^=$-$C_7^=$)		0.5*	1.0*				
Fe/ZrO_2	35.2	15.6	12.6	8.1	30.4	33.3	10.7	3.8	4800	320	2.0	[80]
Fe/Al_2O_3	38.2	12.0	7.6	3.7	26.3	50.4	10.0	7.1				
Fe/CeO_2	22.8	59.0	18.8	15.4	5.5	1.3	1.3	0.4				
Fe/TiO_2	7.7	97.7	0.0	0.0	0.0	2.3	0.0	0.0				

*C_2–C_7 olefins yield and O/P ratio for C_2–C_7 hydrocarbon products.

assumed that decomposing EDTA can produce additional reducing gas, facilitating iron oxide reduction. At the same time, EDTA-2Na weakens iron-support interaction via complexation, thereby inhibiting catalyst sintering. It also promotes the interaction between Fe, Co, and Na, which increases light olefins fraction in the product distribution. Table 7 summarizes the performance data for the Al_2O_3-supported Fe-based catalysts that were discussed.

5.2 | ZrO_2-Supported Fe-Based Catalysts

ZrO_2 attracts attention as a supporting material for heterogeneous CO_2 conversion catalysts thanks to its advantageous thermal, electrical, optical, and co-catalytic properties. Moreover, being a p-type semiconductor, ZrO_2 readily generates oxygen vacancies (OV) and can facilitate CO_2 destructive sorption and promote interactions between active components [88–90]. Ding et al. [91, 92] showed that the ZrO_2-supported Fe-Co-K catalyst (R-FCKZr) is significantly more active than the unsupported one (R-FCK). In this case, the ZrO_2-supported catalyst had a much lower surface area but provided many OVs for the dissociative CO_2 sorption. As a result, enhanced CO production and decreased CH_4 selectivity were achieved. Moreover, the ZrO_2-supported R-FCK catalyst produces olefins more actively than the Al_2O_3-supported analog thanks to its higher surface OV and −OH group density, facilitating carbonate and carboxylic intermediates formation (Figure 9A).

The catalytic performance also depends on the type of crystal phase of ZrO_2. So, Gu et al. [90] showed that monoclinic ZrO_2 (m-ZrO_2) produces OV more readily than tetragonal tetragonal t-ZrO_2. It makes m-ZrO_2 the preferred support phase for Fe-based catalysts. As was shown, ZrO_2 exhibited its activity in the CO_2 hydrogenation reaction, but

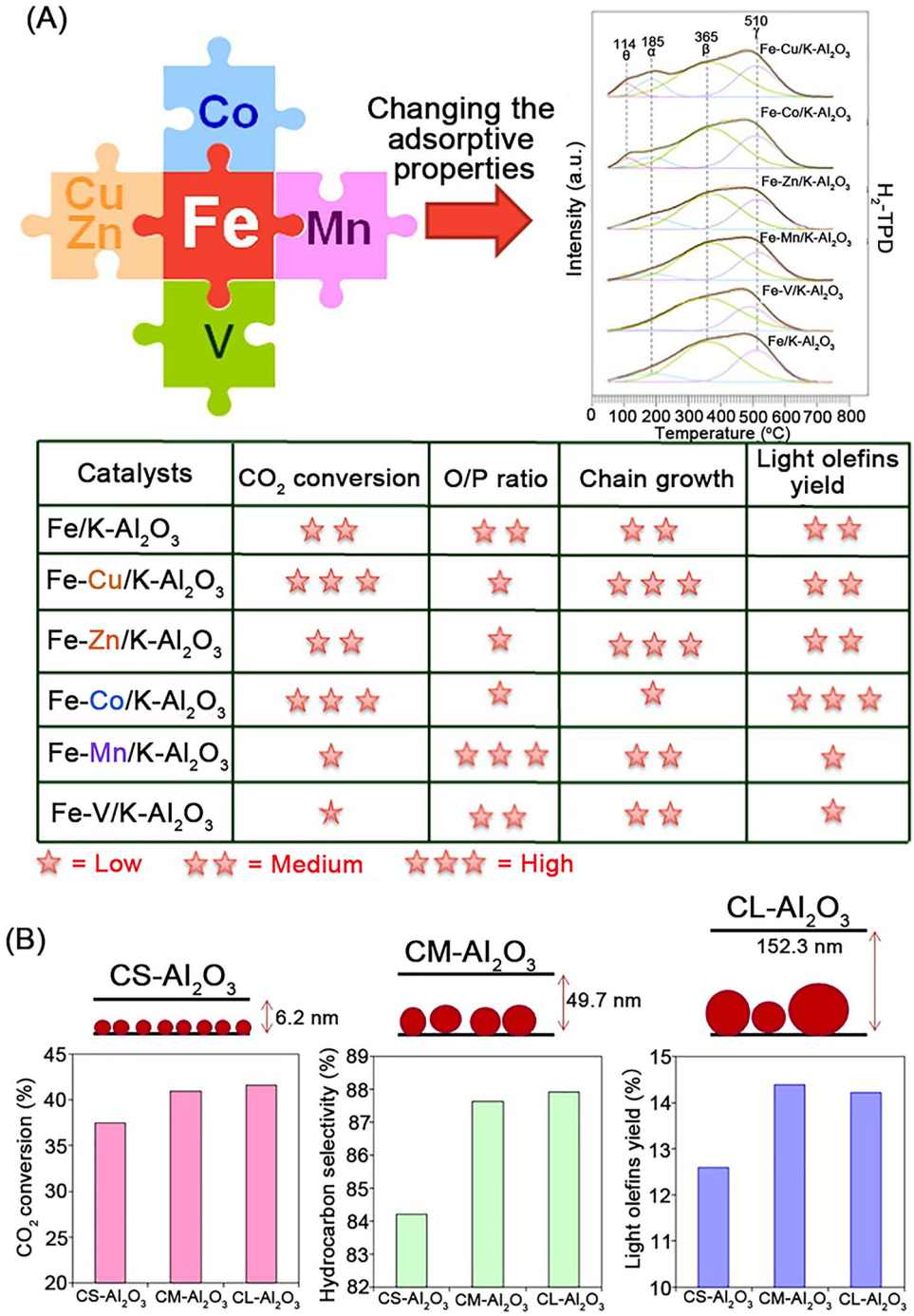

FIGURE 8 | (A) Effect of transition metal promoters on the Fe/K-Al_2O_3 catalyst performance. Reproduced with permission: Copyright 2021, Elsevier [85]. (B) Effect of Al_2O_3 support pore size on the Fe-Co/K-Al_2O_3 catalyst performance. Reproduced with permission: Copyright 2019, Elsevier [84].

CO was the predominant product (86.9% CO selectivity at 26.1% CO_2 conversion).

The addition of Fe alters the composition of the product mixture by increasing the overall hydrocarbon fraction, particularly enhancing light olefins formation. Among the compositions studied, the maximal light olefin selectivity was reached at 10 wt% Fe in the catalyst (14.9% at 40.5% CO_2 conversion). At the same time, further iron addition decreased the O/P ratio and CO_2 conversion value. In the study [94], the dynamic evolution of iron-zirconia catalysts was investigated. The 15% Fe-K/m-ZrO_2 catalyst exhibited both the best CO_2 conversion (38.8%) and selectivity for light olefins (34.3%). The enhanced activity of the Fe-containing species was attributed to the increased surface OV on m-ZrO_2 and the electron-donating properties of the iron, which facilitated better charge transfer between Fe and the ZrO_2 support.

Zhao et al. [35] fabricated K-modified Co-Fe/ZrO_2 catalysts. They demonstrated that support-stabilized defective FeO_x species can act as the main active phase for light olefin production thanks to its enhanced CO_2 and CO binding as well as facilitated H_2 dissociation

TABLE 7 | Al_2O_3-supported Fe-based catalysts for CO_2 hydrogenation into light olefins.

Catalyst	CO_2 conv. (%)	Product selectivity (%)					light olefin yield (%)	O/P	Reaction conditions			Ref.
		CO	CH_4	C_2^0-C_4^0	$C_2^=$-$C_4^=$	C_{5+}			*GHSV* (ml g^{-1} h^{-1})	*T* (°C)	*P* (MPa)	
Fe-Co/K-Al_2O_3 (MH)	59.3	11.7	30.1	6.4	41.3	10.4	24.5	6.4	9240	360	2.0	[87]
Fe-Co/K-Al_2O_3 (C)	54.0	16.0	26.5	6.2	40.7	10.5	22.0	6.6				
0.58%Zn-Fe-Co/K-Al_2O_3	46.5	N/A	N/A	~12	37.0	N/A	17.2	~3	9000	340	2.5	[36]
C3 (Fe-Co-K-Al oxides)	42.2	6.2	N/A	N/A	39.3	N/A	16.6	N/A	3600	350	3.0	[86]
Fe-Co/K-Al_2O_3	40.0	12.2	21.8	6.9	40.5	18.6	16.2	5.9	7200	340	2.0	[85]
Fe-Mn/K-Al_2O_3	29.4	20.2	14.9	5.2	38.8	20.8	11.4	7.4				
F-600	41.4	14.8	18.5	5.4	38.2	23.0	15.8	7.1	7200	320	2.0	[83]
F-700	37.6	24.5	13.8	4.3	33.0	24.4	12.4	7.6				
CL-Al_2O_3	41.6	12.1	28.3	5.3	36.2	18.1	15.1	6.8	7200	320	2.0	[84]
CM-Al_2O_3	41.0	12.4	29.6	5.6	36.0	16.4	14.8	6.4				
$Na_{7.5}$-Fe-Co	32.8	8.1	12.6	4.5	29.9	44.9	9.8	6.6	6000	350	3.0	[44]

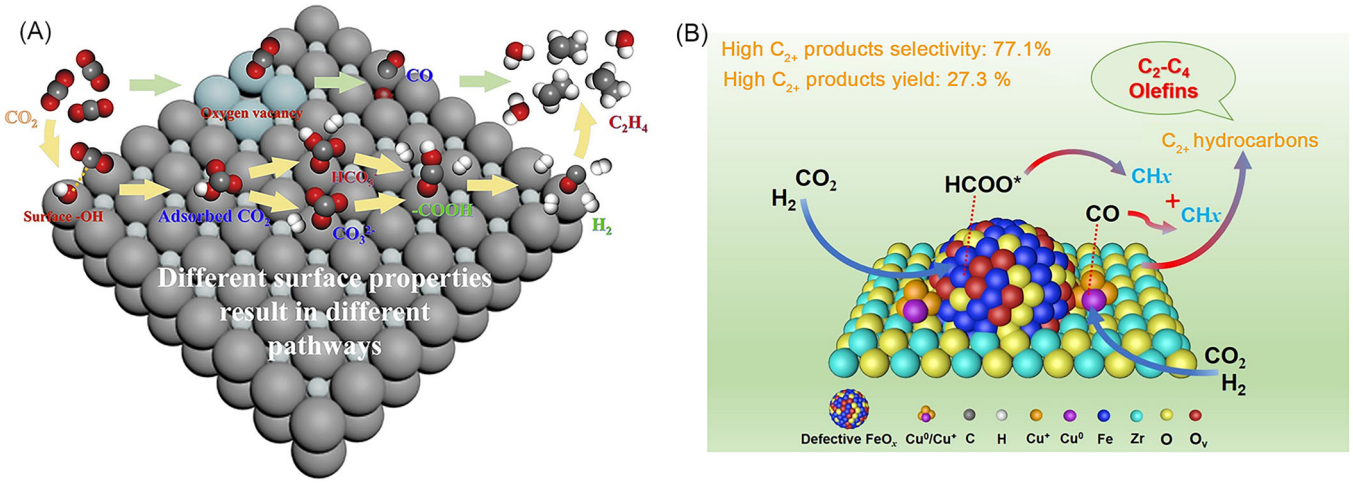

FIGURE 9 | Schematic mechanism of CO_2 hydrogenation (A) over the R-FCKZr catalyst (Reproduced with permission: Copyright 2020, Elsevier [92]) and (B) over the 0.2-CuFe/ZrO_2 catalyst (Reproduced with permission: Copyright 2024, Elsevier [93]).

abilities. Among the compositions studied, 0.3Co-Fe/ZrO_2 exhibited the best performance (34.7% of light olefin selectivity at 48.9% CO_2 conversion). Xu et al. [95] also emphasized the importance of strong interactions between an active Fe-based component and ZrO_2-support. In their study, the MOF-derived Fe_2O_3@ZrO_2 sample showed enhanced activity and higher light olefin selectivity than the mechanically mixed one. In the latter case, separate ZrO_2 species overly increased CO_2 adsorption producing C_{5+} hydrocarbons predominantly. In contrast, strong iron oxide–support interactions optimized the CO_2 adsorption ability of the MOF-derived sample. They also formed electron-rich iron oxide species that were more easily reduced and carburized. The electronic structure of the surface FeO_x species can also be modified with copper oxide incorporation [93]. It was shown that the close proximity between highly dispersed Cu species and iron oxide particles can promote the formation of Cu-Fe_3O_4 interfaces on ZrO_2 instead of Cu-Fe_xC ones while iron carbide phases shaping in the interior of the Fe-Cu/ZrO_2 catalyst (Figure 9B). A small amount of copper oxide species facilitates reactions involving the CO intermediate and accelerates C–C coupling. However, adding too much Cu increases the fraction of long-chain hydrocarbons. The optimal light olefin selectivity (32.6% at 29.8% of CO_2 conversion) was achieved for the 0.2-CuFe/ZrO_2 catalyst.

Li et al. [96] compared Fe-Co-Zr polymetallic fibers and impregnated FeCo/ZrO_2 catalyst. They showed that the strong interactions between metal species in the electrospun fibers provided better dispersion and effective sintering resistivity. Moreover, this synergy also contributed to higher CO_2 conversion and light olefin selectivity.

The study [97] revealed that combining ZrO_2 with a small amount of CeO_2 increases both CO_2 conversion over the K-Fe/ZrO_2 catalyst and light olefins selectivity by enhancing surface basicity and restraining iron oxide crystallites growth. Additionally, the CeO_2 and ZrO_2 combination offers improved thermal and mechanical stability compared to the individual oxides. Moreover, this mixed-oxide support produces surface OV more easily [98, 99]. The principal performance values for the ZrO_2-supported iron catalysts are summarized in Table 8.

5.3 | Carbon Materials Supports

Carbon supports also can offer essential benefits for Fe-based catalysts of CO_2 hydrogenation to light olefins. Among them, we can highlight active phase distribution, pore size control, structurization, and spatial tuning of the active site. In this chapter, a detailed consideration of carbon-supported Fe-based catalysts is proposed. For instance, K. P. de Jong's group [100] studied synthesis gas conversion into light olefin. The authors achieved up to 60 wt% selectivity for light olefin using iron nanoparticle catalysts promoted with sulfur and sodium, dispersed on weakly interactive α-alumina or carbon nanofiber supports. Witoon et al. [101] prepared a series of impregnated Fe-Co-K catalysts over microporous (MC) and micromesoporous (MMC) carbon supports. In both cases, the catalysts exhibited smaller metal oxide particles, enhanced reducibility, activity, and light olefins selectivity compared with the unpromoted catalyst. In particular, the high dispersive metal oxide species inside the micropores of the MC support provided the best CO_2 conversion of about 42%. However, this high dispersity also decreased the number of Fe-K interfacial sites, leading to a predominance of methane production over C_{2+} hydrocarbons. In contrast, the micromesoporous (MMC) support, with slightly lower particle dispersion and CO_2 conversion, provided more Fe-K interfacial sites, resulting in a more selective formation of light olefins. Zhang et al. [37] prepared a series of mesoporous-carbon (MC)-supported Fe-based catalysts, promoted with Zr, W, and Mn. The best results were achieved using the 20%Mn-1.2Fe@MC catalyst (65.7% of C_2–C_6 selectivity at 59.6% of CO_2 conversion). It was shown that catalyst modification essentially affected the C/H ratio over the catalytic surface. In particular, Mn addition enhanced the FeO_x/FeC_x ratio and provided electron transfer to Fe_3C nanoparticles, which inhibited secondary hydrogenation of light olefin formed. The Mn additive also promoted the stability of these species. Another work of the team [30] reported Fe-K@N-OMC (N-doped ordered mesoporous carbon) catalysts, which were modified in another way—via nitrogen incorporation in the mesoporous carbon material. Such N-OMC support had abundant alkaline sites, which enhanced the CO_2 adsorption. Also, it facilitates Fe transformation into FeC_x active phases thanks to Fe ions complexation and their step-by-step transformation into FeN_x and FeC_x. In addition, the K^+ and N atoms increase the electron density by transferring electrons to the Fe active center, which inhibits the adsorption/dissociation of H_2, leading to enhanced selectivity towards light olefins. The proximity of Fe_3O_4 and FeC_x species made this catalyst bifunctional for both CO_2 dissociation into CO and its further transformation into light olefins. The best results in the series were demonstrated for the 0.8Fe-0.1 K@N-OMC catalyst (65.6% light olefins selectivity at 54.5% CO_2 conversion). In the further study [39], different non-metal promoters, such as B, F, P, and Se, were added into mesoporous carbon-supported iron-based catalysts. The F-promoted 0.8Fe@0.28F-MC + 0.02 K catalyst demonstrated the best CO_2 conversion and light olefin selectivity values thanks to easy reducible FeF_2 formation and increased defectiveness of FeO_x species. Moreover, the F-doping enhanced the catalyst stability, inhibiting its sintering and oxidation (Figure 10).

Zhao et al. [102] proposed an expanded graphite (EG)-supported Fe-based catalyst modified with ammonium citrate. This modification improved the dispersity of the iron species and their anchoring on the carbon support, making them more resistant to sintering. In addition, the presence of nitrogen species on the catalyst surface enriched the iron with electrons, thereby facilitating its reduction and carburization. As a result, the catalyst achieved a light olefins selectivity of 37.0% at a CO_2 conversion of 41.8%, along with an increased STY of light olefins. Study [103] describes Na-promoted $CoFe_2O_4$ catalyst, supported on CNT. It was shown that the CNT-supported sample effectively forms joint χ-$(Co_xFe_{1-x})_5C_2$ carbide phase, which makes this catalyst much more efficient in light olefin production than the mechanically mixed one. In this composition, Co containing $x \leq 0.2$ was optimal to obtain the most stable and active catalyst.

TABLE 8 | ZrO_2-supported Fe-based catalysts for CO_2 hydrogenation into light olefins.

		Product selectivity (%)							Reaction conditions			
Catalyst	CO_2 conv. (%)	CO	CH_4	C_2^0-C_4^0	$C_2^=$-$C_4^=$	C_{5+}	light olefin yield (%)	O/P	GHSV (mL g^{-1} h^{-1})	T (°C)	P (MPa)	Ref.
35Fe–7Zr–1Ce–K	57.3	3.1	19.9	7.6	53.6	15.28	30.71	7.08	1000 h^{-1}	320	2.0	[97]
R-FCKZr	39.9	6.3	21.0	17.6	54.4	~0	21.7	3.2	3500 h^{-1}	290	2.0	[92]
0.3-CoFe/ZrO_2	48.9	8.9	16.5	14.5	34.7	25.3	17.0	2.4	4800	320	2.0	[35]
Fe_2O_3@ZrO_2	37.1	19.3	15.7	13.9	36.6	14.5	13.6	2.6	7500	340	3.0	[95]
15Fe−K/m-ZrO_2	38.8	19.9	24.1	10.3	34.3	11.5	13.3	3.3	10,000	320	1.5	[94]
10K13Fe2Co100Zr	~43	N/A	N/A	N/A	27.5	N/A	~12	N/A	7200	400	3.0	[96]
0.2-CuFe/ZrO_2	29.8	22.5	11.5	8.4	32.6	25.0	9.7	3.9	4800	320	2.0	[93]
10Fe-1K/m-ZrO_2	40.5	12.6	65.5	5.9	14.9	~0	6.1	2.6	1200	340	2.00	[90]

Many current studies are devoted to the development of pyrolytic carbon-supported catalysts. So, Chen et al. [104] prepared core-shell FeK@CS(0.5)-py catalyst via iron-chitosan complexes reduction in carbothermal conditions. The ratio of Fe cations to chitosan was identified as a crucial parameter in the synthesis affecting both the surface and the bulk carbide compositions. A higher proportion of the carbide phase was directly correlated with an increased yield of hydrocarbon products. Additionally, the core-shell structure of the FeC_x catalyst was likely to improve its stability over time. In the study [105], FeNaC catalysts were synthesized via thermal decomposition of Fe-Na EDTA salt in different atmospheres (Air, H_2, or N_2). Among the produced materials, the FeNaC-N_2 catalyst demonstrated the best selectivity towards both light and higher olefins. The pronounced olefin productivity was associated with the high dispersity of sodium and iron species within the carbon matrix support, as well as the presence of carboxylates and N-functional groups on the catalyst surface, promoting CO_2 adsorption while suppressing CH_4 and CO byproducts release. Luo et al. [106] constructed a core-shell P-1.2 catalyst via a soft-template technique using phenolic resin as a carbon source and P123 polymer as a template. The produced material consisted of an unpromoted FeO_x-FeC_x core, active in CO_2 hydrogenation reaction, and a thin graphite shell, which prevented the core from sintering and promoted CO_2 adsorption (Figure 11). As a result, 45.1% of light olefin selectivity was obtained at 48.0% CO_2 conversion.

Direct pyrolysis of ferrous fumarate (FF) was applied to prepare iron carbide catalysts in the study [107]. In this case, all the pyrolytic-prepared materials were more active than the impregnated reference sample. It was shown that both low (350°C) and high (600°C) pyrolysis temperatures increase surface disorder and amorphous carbon content, which hindered iron carburization. Among the different process atmospheres, air and hydrogen promote both iron oxides and iron carbides formation, which leads to increased catalytic performance of these samples compared with the under-nitrogen prepared one. Thus, the NaFe-Air-400 catalyst demonstrated the best CO_2 conversion (33.7%) while NaFe-H_2-400 was the most selective towards light olefins (39.9% with $O/P = 6.0$). Jin et al. [38] prepared a series of Fe-based biocarbon-supported catalysts via the thermal treatment of pomelo peel. They showed that the pyrolysis temperature regulated an amount of residual natural oxygen-containing functional groups on the surface of bio-prepared support: lower pyrolysis temperatures saved more of these groups. It resulted in stronger metal-support interactions, increased active phases content, and better performance. So, the Fe/C-400 catalyst demonstrated 47.1% light olefins selectivity at 41.9% of CO_2 conversion and perfect stability during 200 h of the CO_2 hydrogenation reaction.

Metal-organic frameworks (MOFs) can also be used as precursors or sacrificial templates in the pyrolytic synthesis of carbon-supported Fe-based catalysts. For example, Dong et al. [108] prepared a series of carbon-encapsulated Fe-Co/NC materials via pyrolysis of ZIF-67-supported precursors at different temperatures (400°C–700°C). In this case, a nanocarbon (NC) layer was formed, which provided enhanced dispersity of metal particles and promoted their reduction and carburization. Also, it was shown that the MOF pyrolysis temperature significantly affected the catalyst formation by changing many of its characteristics such as active particle size, surface metal loading, and carburization degree. As reported, at least 500°C of pyrolysis temperature is required for effective ZIF-67 pyrolysis and carbon-metal mixing. At the same time, the temperature rising to 700°C led to the excessive carburization of iron-containing species and the largest particle size. As a result, the Fe-Co/NC-600 sample demonstrated the best catalytic outcomes thanks to well iron dispersity within the carbon matrix, better Fe_3O_4/Fe_5C_2 ratio, and Co_2C phase forming. The latter as reported can also be an active site of FTS, promoting CO conversion into hydrocarbons. MOF-derived pyrolytic materials were also reported [109]. In this study, N-doped carbon-coated Fe-based catalysts were synthesized via NH_2-MIL-88B pyrolysis under a nitrogen atmosphere. Two-stage (350°C and 500°C) moderate-temperature calcination was established as optimal pyrolysis conditions providing mild precursor decomposition and resulting in balanced Fe_3O_4-FeC_x structures. In turn, high-temperature calcination led to excessive reduction and carburization. Chen et al. [110] proposed a FeCuNa catalyst obtained via Cu-modified MIL-101(Fe) metal-organic framework pyrolysis. In this study, Na and Cu synergy promoting light olefin formation was revealed. As a result, 34.36% of light olefin selectivity was reached at 42.13% CO_2 conversion. Moreover, the authors proposed a principal mechanism of CO_2 hydrogenation reaction over the FeCuNa catalyst (Figure 12).

Fe-containing MIL-53(Al)-derived catalysts were synthesized and investigated [111]. It was noted that iron oxide crystallite size was an essential factor in producing C_{2+} hydrocarbons from CO_2, and it can be controlled by adjusting the Fe content and promoting the material with another metal. Among the promoters evaluated (Co, Cu, and Zn), Zn was particularly effective for hydrocarbon formation since it promotes CO_2 and H_2 adsorption over the catalytic

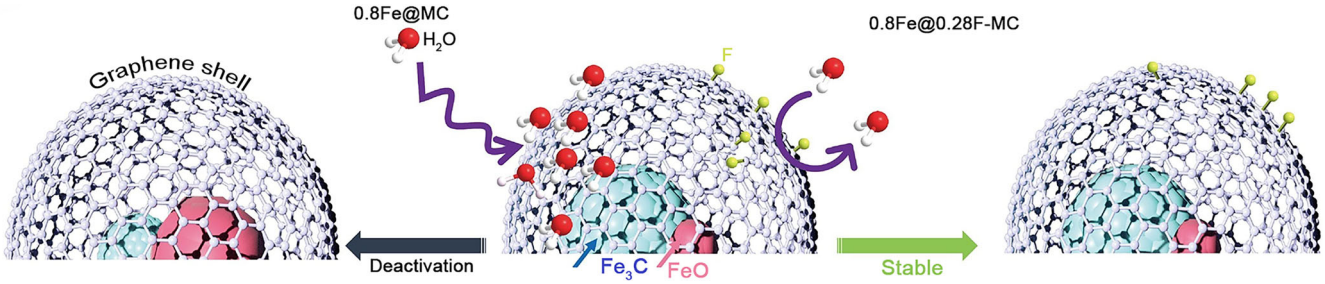

FIGURE 10 | Structure and stability of an active site of MC-encapsulated iron catalysts. Reproduced with permission: Copyright 2023, Elsevier [39].

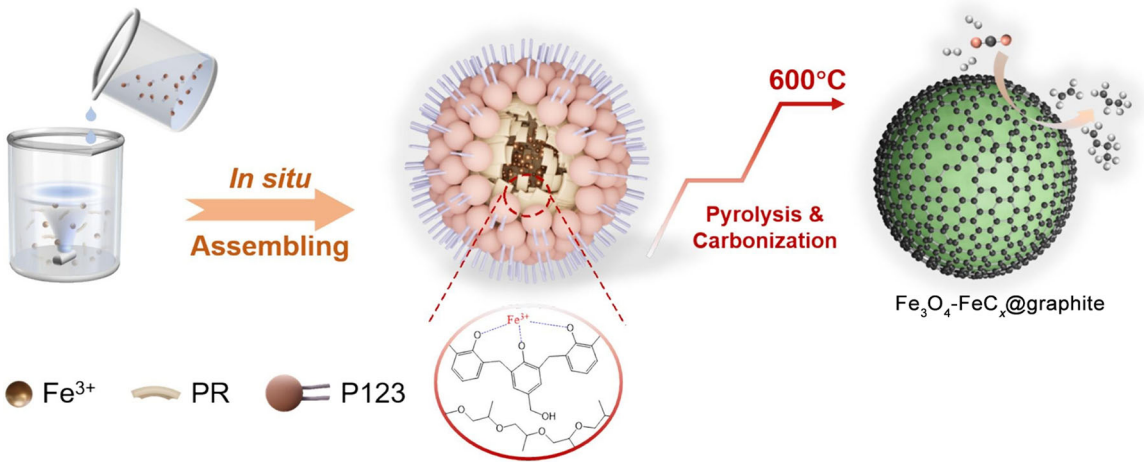

FIGURE 11 | Preparation scheme of the Fe_3O_4-FeC_x graphite-encapsulated catalyst. Reproduced with permission: Copyright 2024, Elsevier [106].

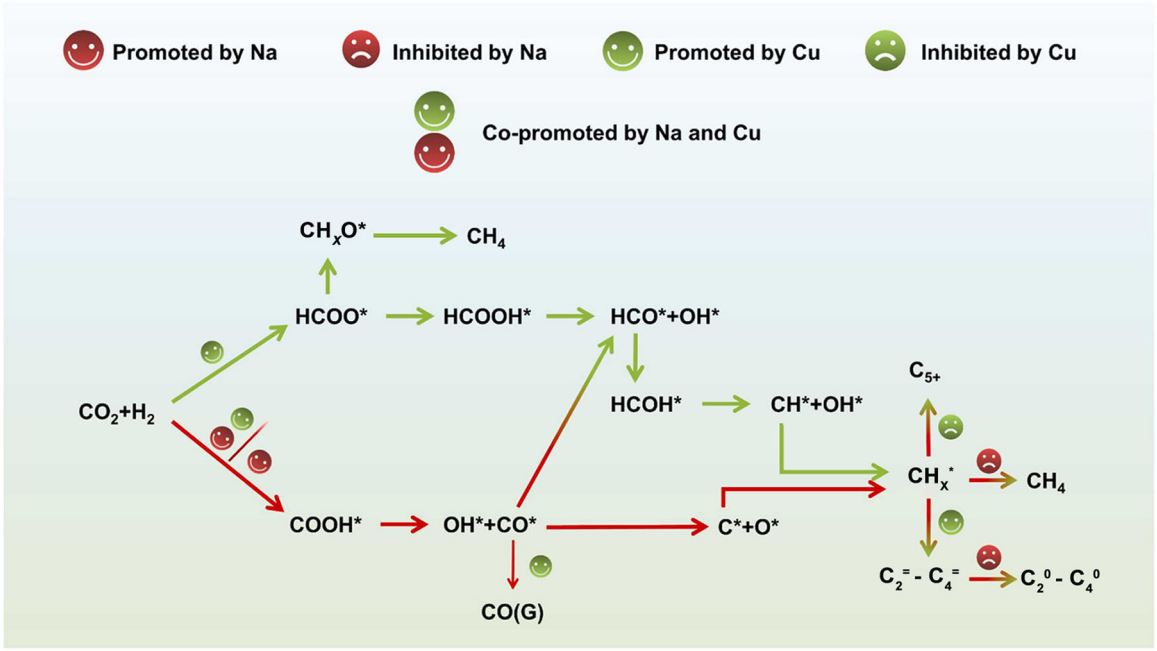

FIGURE 12 | The proposed mechanism of light olefins formation over pyrolytic FeCuNa MOF-derived catalyst. Reproduced with permission: Copyright 2024, Elsevier [110].

surface. In turn, secondary hydrogenation was inhibited with K addition. As a result, 0.15K-0.1Zn-58%$FeAl_{MIL-53}$ showed the best 40.1% of light olefin selectivity at 36.0% of CO_2 conversion.

Liang et al. [112] developed a series of Fe-Co catalysts supported over graphene oxide (GO). They confirmed that joint Fe-Co surface species with a low Co/Fe ratio are responsible for light olefins formation. At the same time, spatial Fe and Co separation and an increase in the Co/Fe ratio intensified the carbon chain growth, resulting in predominant liquefied petroleum (LPG) formation. Thus, the graphene fencing technique, proposed in the study, can be effectively used for fine product distribution tuning (Figure 13). Table 9 presents the performance data of the carbon-supported Fe-based catalysts for CO_2 hydrogenation into light olefins.

5.4 | Zeolite-Modified Fe-Based Catalysts

Zeolites are widely studied and used as catalyst supports and co-catalysts thanks to their highly porous structure, tunable acidity, and good thermal stability. However, combining Fe-based catalysts with zeolites can decrease the selectivity of light olefins due to promoted hydrogen transfer, leading to aromatics and paraffins formation [113]. This may be the reason for the relatively small number of articles presenting mixed iron + zeolites catalysts for light olefin production. Nevertheless, zeolites with decreased acidity, such as SAPO-34, MOR, or alkaline-modified ZSM-5, as well as control of mixed catalysts preparation, can provide several benefits for CO_2 hydrogenation to light olefins, including enhanced active species dispersity and anchoring as well as activating CO_2 sorption and dissociation. Moreover, appropriate zeolite support can also serve as a

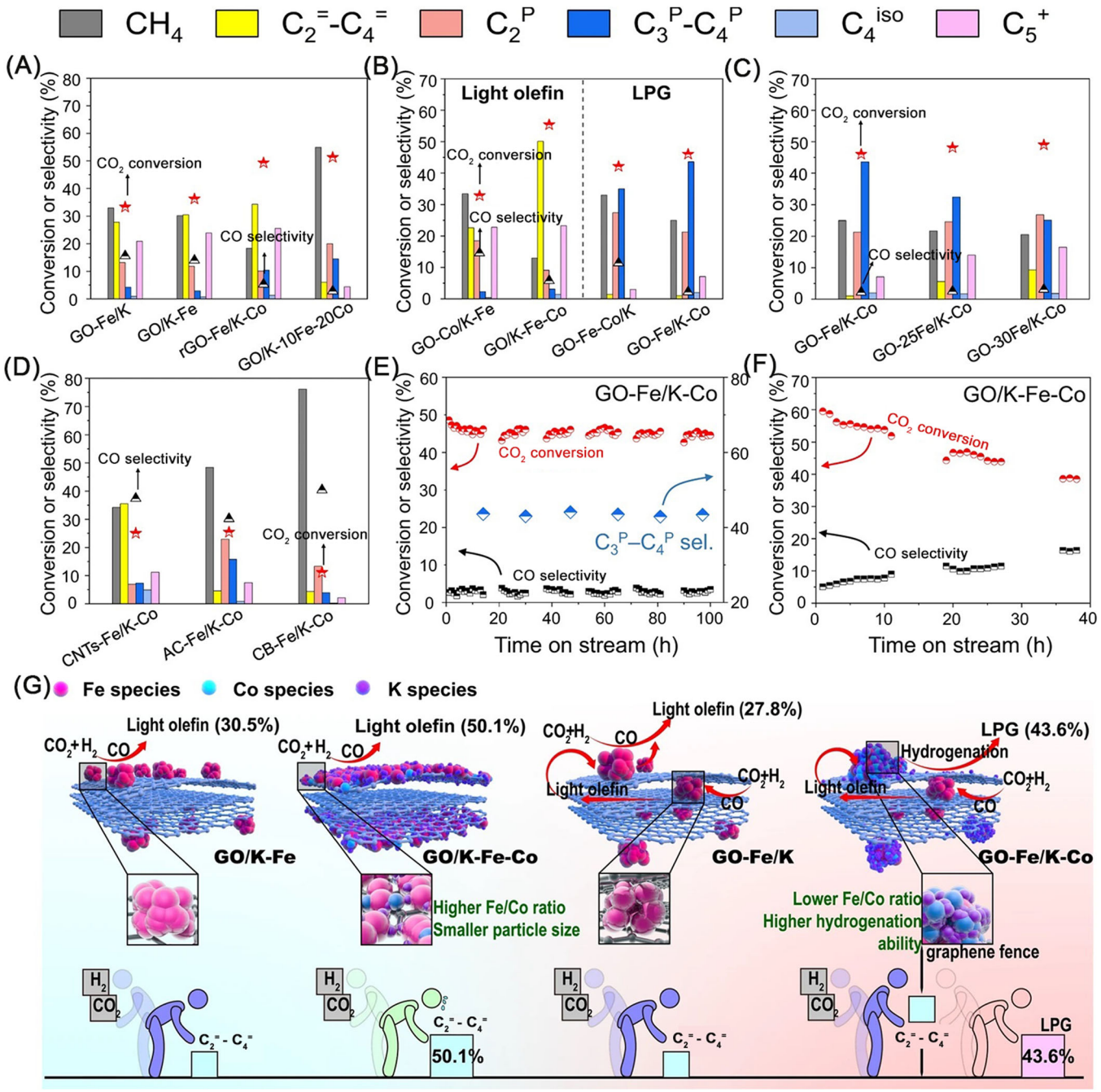

FIGURE 13 | Performance and stability of Fe-based catalysts, prepared via graphene fencing technique. (A-D) CO_2 conversion and product distribution data. (E) The GO-Fe/K-Co catalyst stability. (F) The GO/K-Fe-Co catalyst stability. (G) Schematic representation of the graphene fence-modulated Fe-Co active sites determining product type. Fe, Co, and K species are depicted as red, light blue, and purple spheres, respectively. Characters in different colors denote corresponding active site types. Reproduced under the terms of the CC-BY license (http://creativecommons.org/licenses/by/4.0/): Copyright 2024, The Authors, published by Springer Nature [112].

cocatalyst, promoting the additional methanol-to-olefins (MTO) pathway in addition to RWGS-FTS, thereby overcoming the polymerization kinetics limitations of the latter.

Ding et al. [32] developed a series of Fe-Cu-K + SAPO-34 catalysts. Among them, the $Fe_{0.45}Cu_{0.45}K_{0.10}$/SAPO-34 (R-FCK/-SAPO) catalyst demonstrated the best values of 49.7% CO_2 conversion, 62.9% light olefin selectivity, and STY 4.19 mmol g_{cat}^{-1} h^{-1}. This outstanding performance was explained by several causes, such as the exposure of joint Cu-Fe(100) interface, facilitated reducibility of the catalyst, promoted CO_2 adsorption and dissociation, θ-Fe_3C sites formation, and accelerated reacting gases diffusion. Additionally, a three-pathways mechanism was proposed (Figure 14).

In the study [33], the FeZnK catalyst was prepared and mixed with SAPO-34 in three different ways, which had a noticeable effect on the resulting performance. So, the FeZnK/SAPO-M sample, prepared by joint milling in a mortar, showed the worst activity and light olefins selectivity of less than 2%, which was

TABLE 9 | Carbon-supported Fe-based catalysts for CO_2 hydrogenation into light olefins.

Catalyst	CO_2 conversion (%)	Product selectivity (%)					light olefin yield (%)	O/P	Reaction conditions			Ref.
		CO	CH_4	C_2^0-C_4^0	$C_2^=$-$C_4^=$	C_{5+}			GHSV (mL g^{-1} h^{-1})	*T* (°C)	*P* (MPa)	
0.8Fe-0.1 K@N-OMC	54.5	8.9	9.3	14.0	65.6	2.9	35.8	4.7	4800	320	3.0	[30]
GO/K-Fe-Co	55.4	6.3	12.1	12.7	47.0	21.7	26.0	3.7	4.5 g h mol^{-1}	320	3.0	[112]
P-1.2	48.0	8.2	8.7	14.9	45.1	23.1	21.6	3.0	12,000	320	3.0	[106]
Fe/C-400	41.9	19.6	16.4	5.7	47.1	11.8	19.7	8.2	2000	320	2.0	[38]
0.8Fe@0.28F-MC + 0.02 K	42.6	23.5	3.7	9.1	44.6	18.1	19.0	4.9	12,000	320	3.0	[39]
Fe/EG-1	41.8	10.2	11.0	6.8	37.0	34.9	15.5	5.4	5000	320	3.0	[102]
FeNaC-N_2	36.9	10.7	12.8	6.3	39.6	30.5	14.6	6.3	12,000	320	3.0	[105]
3-NFS-5 (FeCuNa)	42.1	18.1	6.2	5.5	34.4	28.2	14.5	6.3	1500	320	3.0	[110]
0.15K-0.1Zn-58%$FeAl_{MIL-53}$	36.0	29.4	11.6	6.4	40.1	12.5	14.4	6.3	3600	300	1.1	[111]
NaFe-Air-400	33.7	17.2	14.7	7.0	39.0	22.1	13.1	5.5	4000	320	3.0	[107]
NaFe-H_2-400	32.4	13.1	14.3	6.7	39.9	25.7	12.9	6.0				
Na−$CoFe_2O_4$/CNT	34.4	18.6	12.0	4.5	31.6	33.3	10.9	7.0	3600	340	1.0	[103]
60Fe-Co-K/40MMC	39.5	32.2	~40	~5.6	27.2	~11.5	10.7	~4.9	3600	400	2.0	[101]
FeCo/NC-600	37.0	1.1	44.5	20.8	27.1	1.6	10.0	1.3	6240	320	2.0	[108]
Fe/C-K@NC-350/500	35.1	28.1	17.1	5.7	27.1	22.0	9.5	4.8	5000	340	3.0	[109]
20%Mn-1.2Fe@MC	59.6	7.1	7.5	12.3 (C_2^0-C_6^0)	65.6 ($C_2^=$-$C_6^=$)	7.12 (C_{7+})	39.1*	5.3*	12,000	320	3.0	[37]
FeK@CS(0.5)-py	41.0	27.5	14.1	7.5 (C_2^0-C_6^0)	51.0 ($C_2^=$-$C_6^=$)		20.9*	6.9*	6000	330	1.5	[104]

*C_2–C_6 olefins yield and O/P ratio for C_2–C_6 hydrocarbon products.

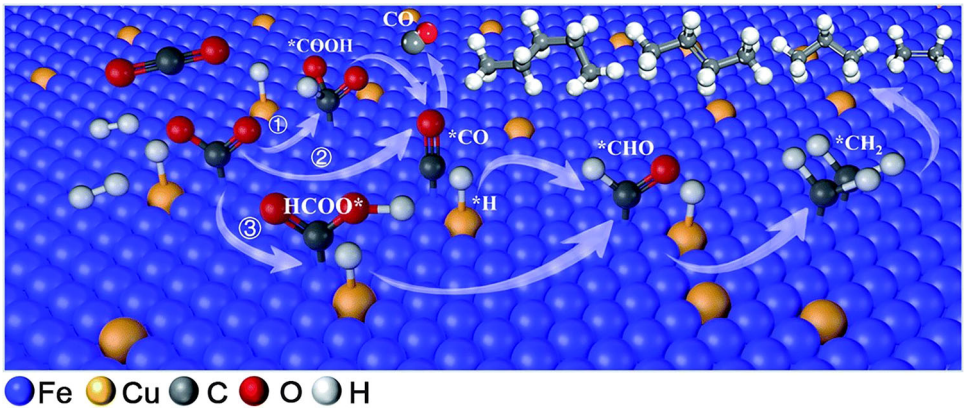

FIGURE 14 | Three-pathways mechanism of CO_2 hydrogenation into light olefins over R-FCK/SAPO catalyst. Reproduced with permission: Copyright 2012, Royal Society of Chemistry [32].

assigned to excessive ions exchange between FeZnK and SAPO-34, dramatically decreasing surface K ions concentration. In turn,

joint shaking of FeZnK and SAPO-34 granules produced the FeZnK/SAPO-G sample with the best activity, light olefin selectivity, and good 72 h stability. In this case, the enhanced performance was attributed not only to a higher surface concentration of potassium ions but also to the ZnO, Fe_3O_4, and χ-Fe_5C_2 active phases formation. Numpilai et al. [114] combined Fe-Co/K-Al_2O_3 with In_2O_3/SAPO-34 in a single catalytic system. They demonstrated that the mixture configuration arrangement critically influences both CO_2 conversion rate and product distribution. Simple physical mixing leads to substantial pore blockage, In_2O_3 reduction, and hydrogen spillover, promoting the excessive hydrogenation of olefins to paraffins. In contrast, a dual-bed configuration with In_2O_3/SAPO-34 positioned upstream of Fe-Co/K-Al_2O_3 (the T-InS/B-FeCo catalytic system) achieved significantly improved performance. In this arrangement, the front bed selectively converts CO_2 into light olefins, while the downstream bed further transforms the residual CO_2 into additional olefins, collectively achieving a 21.5% yield. However, reversing the bed order compromises performance, as the subsequent In_2O_3/SAPO-34 bed tends to hydrogenate the olefins formed over Fe-Co/K-Al_2O_3, lowering the olefin yield to 16.2%. Oni et al. [42] proposed a Y_2O_3/Fe-Co/SAPO-34 catalyst. This micro-mesoporous composite material combines both acid and basic sites on its surface while dispersed metal particles are uniformly distributed within SAPO-34. In turn, defective Y_2O_3 increases basicity and facilitates CO_2 dissociation. As a result, 53.9% of light olefin selectivity was achieved; however, CO_2 conversion was only 19.9%.

According to one study [115], the Fe_2O_3@KO_2/MOR catalyst demonstrated 33.2% of light olefins selectivity at 47.1% of CO_2 conversion. In this case, the zeolite surface can efficiently link CO intermediate into formate species with further hydrogenation, decreasing CO fraction in the product mixture with additional light olefin production. Also, MOR replacement with ZSM-5 leads to the intensive formation of aromatic compounds. However, the acidity of ZSM-5 can be modified to increase light olefins selectivity. So, in the study [116], zeolite was impregnated with calcium nitrate, and the sample containing 6 wt% calcium was found to be optimal for light olefins production. As a result, combined Fe_2O_3@KO_2 + Ca-ZSM-5 catalyst (6Ca_Z) demonstrated 37.9% of light olefin selectivity at 46.6% of CO_2 conversion. In the work [117], a multifunctional Fe_2O_3@KO_2/ZrS/SAPO-34 catalyst was prepared. As reported, the Fe_2O_3@KO_2 component was responsible for RWGS and FTS processes while SAPO-34 zeolite linked CO intermediate. In turn, ZnS cracked C_{5+} products, further increasing the light olefins fraction in the product distribution. As a result, about 24% of light olefin yield was reached. Table 10 summarizes the performance data of the zeolite-modified Fe-based catalysts for CO_2 hydrogenation to light olefins.

6 | Other Two-Component and Multi-Component Fe-Based Catalysts

In the previous chapters, we have considered the most discussed compositions of Fe-based catalysts for light olefins production via CO_2 hydrogenation. At the same time, current research offers a wide diversity of catalysts, which is challenging to classify consistently. For that reason, we propose discussing such compositions in this special chapter.

Cai et al. [118] investigated the effects of Mn and Al promotion on a $CaCO_3$-supported Fe-based catalyst. Their findings revealed that these modifications increased the Fe_3O_4/FeC_x ratio, with the simultaneous addition of both promoters being the most effective. Consequently, the fraction of light olefins increased while the proportion of C_{5+} products decreased. Nevertheless, the higher product fraction was still predominant, and the best achieved light olefins selectivity was 13.3% at the 35.9% CO_2 conversion. Another work [119] investigates K/La-$FeBO_3$ perovskite catalysts (where B = Zn, Ni, Mn, Al, Zr, or Cu). It was shown that incorporating either Cu or Zn into these catalysts significantly increases lattice oxygen mobility, which in turn facilitates CO_2 adsorption and enhances its conversion. However, the K/$LaFeCuO_3$ sample predominantly produced CO, whereas only the K/$LaFeZnO_3$ catalyst mainly yielded light olefins, demonstrating 30.5% light olefin selectivity at 48.5% CO_2 conversion. In the study [120], a 3D-printing approach was adapted to prepare a monolithic spiral-organized Na-Fe@C-3D-spi catalyst. Developed pore structure, and optimized mass and heat transfers, as well as electron-rich surface, provided 37.2%

TABLE 10 | Zeolite-modified Fe-based catalysts for CO_2 hydrogenation into light olefins.

Catalyst	CO_2 conversion (%)	Product selectivity (%)					light olefin yield (%)	Reaction conditions				Ref.
		CO	CH_4	C_2^0-C_4^0	$C_2^=$-$C_4^=$	C_{5+}		O/P	GHSV (ml g^{-1} h^{-1})	*T* (°C)	*P* (MPa)	
R-FCK/SAPO	47.5	9.7	14.6	8.8	62.9	2.3	29.9	7.2	1500	330	1.5	[32]
T-InS/B-FeCo	48.0	4.0	25.9	9.6	44.8	15.8	21.5	4.7	3000	360	2.5	[114]
FeZnK/SAPO-G	49.4	23.4	12.7	5.9	40.1	17.8	19.8	6.9	4500	320	1.5	[33]
Fe_2O_3@KO_2/ZrS/SAPO-34	49.0	13.0	N/A	N/A	42.0	N/A	19.0	N/A	5000	375	3.0	[117]
6Ca_Z	46.6	13.0	14.4	4.6	37.9	30.0	17.7	8.2	5000	375	3.0	[116]
Fe_2O_3@KO_2/MOR	47.1	12.9	13.7	N/A	33.2	N/A	15.6	N/A	5000	375	3.0	[115]
Y_2O_3/Fe-Co/SAPO-34	19.9	34.7	1.4	12.6	53.9	N/A	10.7	4.3	10,000	400	2.0	[42]

light olefin selectivity at 32.4% CO_2 conversion. Elishav et al. [121] developed an electrospinning technique for K/Fe-Al-O nanobelts production. This well-structured material with good dispersion of potassium provided 52% of C_2–C_5 olefins selectivity at 48% of CO_2 conversion. Zhang et al. [122] showed that FeNa-catalyst doping with Ce enhances both CO_2 conversion and hydrocarbon formation. At the same time, this results in additional methanation and decreasing in light olefins selectivity. They also demonstrated that replacing the pre-reduction atmosphere from H_2 to CO resulted in lower CO selectivity and a higher fraction of light olefins in the product mixture. This effect was attributed to increased Fe_3O_4/Fe_xC_y and Na/Fe surface ratios, along with less concentration of surface OV associated with enhanced CO formation. At the same time, Guo et al. [123] reported that minor Ce introduction (Ce/Fe = 1/99) enhanced light olefin selectivity while methane formation was inhibited. This effect was explained by promoting CO* and CH_x* intermediates formation and Fe_3O_4 phase generation. However, further Ce content increases CO production due to simultaneous (1) rapid CO generation over OV and (2) inefficient hydrocarbon formation due to strong Fe-Ce interactions suppressing FTS-active iron carbides phases formation. In one work [124], hierarchical β-Mo_2C was synthesized and promoted with Fe. Although CO_2 conversion did not exceed 10% in any conditions studied, this combined catalyst demonstrated outstanding 79.4% ethylene selectivity at 300°C and 92% at 400°C. Wang et al. [125] suggested K-Fe-Ti layered metal oxide (LMO) system. This structure is characterized by a low surface area, which complicates FeO_x species reduction and carburization. However, acid treatment creates many vacancies and develops the catalyst's structure. It resulted in a much better light olefins selectivity (59.3% in the hydrocarbon mixture and O/P ratio = 7.3) for the 0.8K-2.4Fe-1.3Ti catalyst. Nevertheless, CO selectivity was 70.1% in this case. In the further study of the authors [126], the K-Fe-Ti LMO structure was modified by replacing part of Fe with Zn. Although no evident trends are progressing with the increase in Zn content, several tendencies can be noted. Firstly, adding any amount of Zn in the studied range (0.2–0.5 in Zn/Fe ratio) leads to a dramatic decrease in CO_2 conversion (from 35.2% to 13.0%). At the same time, CO formation is significantly suppressed, which increases the hydrocarbon product fraction. As a result, the best light olefins selectivity (23.6% and O/P = 6.5) was achieved at the Fe/Zn ratio of 2. At the same time, better O/P ratio was reported to Fe/Zn = 4 while light olefins selectivity remained relatively high (21.7% and O/P = 7.1). Another paper [127] reports layered double-hydroxide (LDH) derived Fe-Co bimetallic catalysts based on MgO. In this case, the high CO_2 conversion of 40.6% and light olefin selectivity of 36.4% were reached thanks to the pronounced CO_2 adsorption over the MgO support and the synthetic way providing strong interactions between Fe and Co, forming joint $Co_xFe_{5-x}C_2$ species. Sun et al. [128] developed a K/$La_{0.4}Co_{0.4}$-$Fe_{0.6}O_3$ oxygen carrier for CO_2 hydrogenation. They demonstrated that the reaction proceeds via a dual mechanism. In this case, Co-promoted defective lanthanum oxide species enhance conversion into formate species while bimetallic Co-Fe species (first of all, Co_7Fe_3) catalyze the FTS process. Zhao et al. [129] reported a K-promoted trimetallic Fe-Co-Ni catalyst providing both excellent CO_2 conversion of 47.5% and light olefin selectivity of 46.8%. This performance was explained by an appropriate Fe_3O_4/Fe_5C_2 ratio, developed pore structure, and alkali metal promotion. In the study [130], a serial of Fe-M (M = Co, Mn, Cu, Zn) double metal cyanide catalysts was prepared. Among these compositions, the Fe-Co (R) catalyst showed the best light olefin selectivity thanks to enhanced CO_2 and CO adsorption ability promoting their conversion into hydrocarbons. At the same time, this catalyst demonstrated the lowest O/P ratio due to enhanced H_2 adsorption and secondary hydrogenation of the light olefins formed. In contrast, the Fe-Mn (R) catalyst demonstrated the best O/P ratio among the serial since its weaker H_2 sorption ability. However, it is also less active in the adsorption of carbon oxides, which leads to the lowest CO_2 conversion ratio and the highest CO fraction in the product distribution. Table 11 summarizes the performance data achieved using the catalysts discussed in this chapter.

7 | Photothermal Conversion of CO_2 Into Light Olefins Over Fe-Based Catalysts

Photothermal catalysis, combining the photo- and thermochemical effects of sunlight, offers an alternative approach to driving chemical reactions by enhancing reaction rates and altering selectivity patterns under moderate conditions [131]. Additionally, photothermal catalysts demonstrate exceptional

TABLE 11 | Two-component and multi-component catalysts for CO_2 hydrogenation into light olefins.

Catalyst	CO_2 conversion (%)	Product selectivity (%)					light olefin yield (%)	O/P	Reaction conditions			Ref.
		CO	CH_4	C_2^0-C_4^0	$C_2^=$-$C_4^=$	C_{5+}			GHSV (mL g^{-1} h^{-1})	*T* (°C)	*P* (MPa)	
FCN-K(a)	47.5	7.3	17.0	23.5	46.7	5.4	22.2	2.0	11,040	320	1.0	[129]
1CeFe	42.8	14.9	29.2	4.4	35.2	16.3	15.1	8.0	10,000	320	1.5	[123]
Fe—Co (R)	39.1	13	31.0	6.9	38.1	10.0	14.9	5.5	3600	320	2.0	[130]
FeCo-9:1-LDH	40.6	9.6	18.0	10.4	36.4	22.3	14.8	3.5	7200	320	3.0	[127]
$K/LaFeZnO_3$	48.5	25.7	11.6	12.6	30.5	19.7	14.8	2.4	1000 h^{-1}	320	2.0	[119]
Na-Fe@C-3D-spi	32.4	29.3	17.5	6.9	37.2	9.0	12.1	5.4	24,000	320	3.0	[120]
$K/La_{0.4}Co_{0.4}Fe_{0.6}O_3$	36.0	16.4	40.1	13.0	24.5	5.9	8.8	1.9	1000 h^{-1}	320	2.0	[128]
Fe10Mn2Al10Ca	35.6	32.2	5.8	2.0	13.3	46.7	4.8	6.6	12,000	320	3.0	[118]
0.8K-2.4Fe-1.3Ti	35.2	70.1	5.2	1.8	13.3	2.1	4.7	7.3	1000 h^{-1}	320	2.0	[125]
0.8K-1.92Fe-0.48Zn-1.3Ti	14.6	53.6	8.0	3.0	21.7	8.9	3.2	7.1				[126]
0.8K-1.6Fe-0.8Zn-1.3Ti	13.0	49.1	9.2	3.6	23.6	9.7	3.1	6.5				
K/Fe-Al-O nanobelts	48.0	16.0	10.0	5 (C_2^0-C_5^0)	52.0 ($C_2^=$-$C_5^=$)	12 (C_{6+})	25*	10.0	$WHSV_{CO2} = 1$ h^{-1}	300	1.0	[121]
FeNa•0%Ce	35.2	10.4	32.7	7.7 (C_2^0-C_6^0)	46.2 ($C_2^=$-$C_6^{=)}$	3.0 (C_{7+})	16.3**	6.0	9000	320	2.0	[122]
FeNa•1%Ce	39.7	8.0	40.2	9.8 (C_2^0-C_6^0)	39.8 ($C_2^=$-$C_6^=$)	2.0 (C_{7+})	15.8**	4.0				
Fe(0.5)-Mo_2C	9.8	0.5	2.1	4.3 (C_2^0-C_3^0)	92.0 (C_2H_4)	N/A	9.0***	N/A	N/A	400	4.0	[124]

*C_2–C_5 olefins yield and O/P ratio for C_2–C_5 hydrocarbon products.
**C_2–C_6 olefins yield and O/P ratio for C_2–C_6 hydrocarbon products.
***Ethylene yield.

sunlight utilization efficiency, effectively harnessing nearly the entire solar spectrum, including ultraviolet (UV), visible, and infrared (IR) light [132]. Since its proposal in 2014, photothermal catalysis has rapidly advanced, garnering attention for its ability to integrate into industrial processes and enabling various reaction systems like CO_2 hydrogenation, RWGS, methane dry reforming, and FTS-related processes [133, 134]. By utilizing solar energy, it facilitates the production of renewable solar fuels such as CO, CH_4, CH_3OH, syngas, higher hydrocarbons, and light olefins, offering a sustainable alternative to fossil fuels and addressing critical energy and environmental challenges. Light olefins are predominantly produced through the steam cracking of light hydrocarbons like naphtha, a highly energy-intensive and CO_2-emitting process that releases over 180 Mt of CO_2 annually (Figure 15IA). In contrast, the photothermal catalytic hydrogenation of CO_2 using sunlight offers a sustainable alternative, enabling the production of high-value light olefins with minimal carbon emissions when hydrogen is sourced from renewable energy (Figure 15IB–C) [135].

Intensive efforts have focused on advancing photothermal industrialization, with large-scale solar systems like heliostat fields and towers envisioned to deliver high-temperature conditions for driving fuel production and traditional industrial processes [137]. Compared to thermocatalysis, photothermal catalysis not only reduces fossil energy consumption but also modifies the electronic structure of catalysts under sunlight, enhancing CO_2 reduction selectivity. While photocatalysis can convert CO_2 without H_2, photothermal CO_2 hydrogenation offers distinct advantages, including nearly 100% sunlight absorption by narrow- or zero-band-gap materials and an ultrahigh CO_2 conversion rate exceeding 100 mmol g^{-1} h^{-1}, making it a promising candidate for industrial applications [132, 138].

Among the various metal-based photothermal catalysts, Fe-based catalysts have garnered widespread attention in the RWGS reaction due to their abundant earth resources, relatively low cost, high CO_2 conversion rate, and superior photothermal conversion efficiency, making them ideal for photothermal CO_2 conversion with excellent catalytic activity and selectivity [132, 138, 139]. Fe-based catalysts, featuring versatile operating conditions and adaptable product distribution, uniquely integrate reactive sites for both the RWGS and FTS, where the active phases Fe_3O_4, Fe_3C, and Fe_5C_2 play a critical role in ensuring stability, equilibrium, and synergism between the reaction steps, thereby enabling controllable chain growth and achieving high olefin selectivity (Figure 15II) [135, 136, 139].

For instance, Song et al. [136] developed Fe-based catalysts (Fe_3O_4; Fe_3O_4 + Fe; Fe; Fe_3C + Fe; Fe_3C) through hydrogenation/carbonization of Fe_3O_4 to achieve tunable selectivity in the photothermal conversion of CO_2 (Figure 16I). The authors demonstrated full selectivity toward CO (100%) with Fe_3O_4 and high hydrocarbon selectivity (> 97%) with θ-Fe_3C, achieving activities of 11.3 mmol g^{-1} h^{-1} and 10.9 mmol g^{-1} h^{-1}, respectively, while highlighting the role of nonthermal effects in enhancing catalytic performance. Later, the same group [135] investigated solar-driven CO_2 hydrogenation to produce light olefins, addressing the challenge of C-C coupling in photothermal catalytic processes. Using a K-promoted Ru/Fe_3O_4 catalyst, the authors achieved a production rate of 0.63 mmol g^{-1} h^{-1} and an O/P ratio of 10.2, with Ru-FeO_x interfaces playing a crucial role in C–C bond formation and photochemical contributions enhancing CO_2 activation and olefin selectivity (Figure 16II). The direct interaction at the Ru/Fe_3O_4 interface is crucial for C_{2+} product formation, with olefin production enhanced by alkali metals like K or Na under irradiation, while alternative metals or supports fail to achieve similar results. It has been confirmed that photothermal catalysis exhibits distinctly different performance compared to thermal catalysis over the K-Ru/Fe_3O_4 catalyst at the same catalyst bed temperature (Figure 16IIC), highlighting the significant role of the photochemical contribution in the photothermal reaction process. Furthermore, the K-Ru/Fe_3O_4 catalyst exhibits excellent stability, maintaining consistent light olefins selectivity and high CO_2 conversion over 10 cycles. Under natural sunlight, it achieves an impressive light olefins selectivity of 49.3% with an O/P ratio of 12.3, underscoring its potential for efficient CO_2 hydrogenation to lower olefins without the need for external energy input.

8 | Mechanistic Aspects of CO_2 Hydrogenation Over Fe-Based Catalysts Into Light Olefins

Preparation of Fe-based catalysts from available raw materials usually results in Fe_2O_3. However, this iron oxide does not show significant activity in the CO_2 hydrogenation reaction [140]. For this reason, catalyst pre-reduction in H_2 or CO flow is a widespread practice. The reduction process is stepwise following the sequence:

$$Fe_2O_3 \rightarrow Fe_3O_4 \rightarrow FeO \rightarrow Fe$$

Although complete reduction of iron oxide species requires relatively high temperatures (> 600°C) [141], the noteworthy fact is Fe_3O_4 activity in the RWGS reaction [142–144]. Because of that, the pre-reduction stage is often performed in mild conditions. Although a certain amount of metallic iron forms, the CO_2-FTS conditions make this phase unstable, primarily due to high CO_2 and H_2O concentrations [19]. Then, during the CO_2 hydrogenation reaction, adsorbed carbon species (C*) can diffuse into the iron oxides matrix and form iron carbides phases, such as θ-Fe_3C, ε-Fe_2C, χ-Fe_5C_2, and others [145, 146]. Afterward, these iron carbides can oxidize if water and CO_2 contents predominate over hydrogen and CO contents. The iron carbide phases (especially Hägg iron carbide χ-Fe_5C_2) are recognized as the main active species for the Fischer–Tropsch hydrocarbon synthesis, so their reoxidation is usually undesirable. Since the main catalytic phases formation occurs in situ during the CO_2 hydrogenation, this phenomenon is named "selforganization of the catalyst" [147]. The complete scheme of iron phases transformations is presented in Figure 17A.

The schematic mechanism of CO_2 hydrogenation is demonstrated in Figure 17B. As outlined earlier, CO_2 hydrogenation over Fe-based catalysts begins with the RWGS reaction:

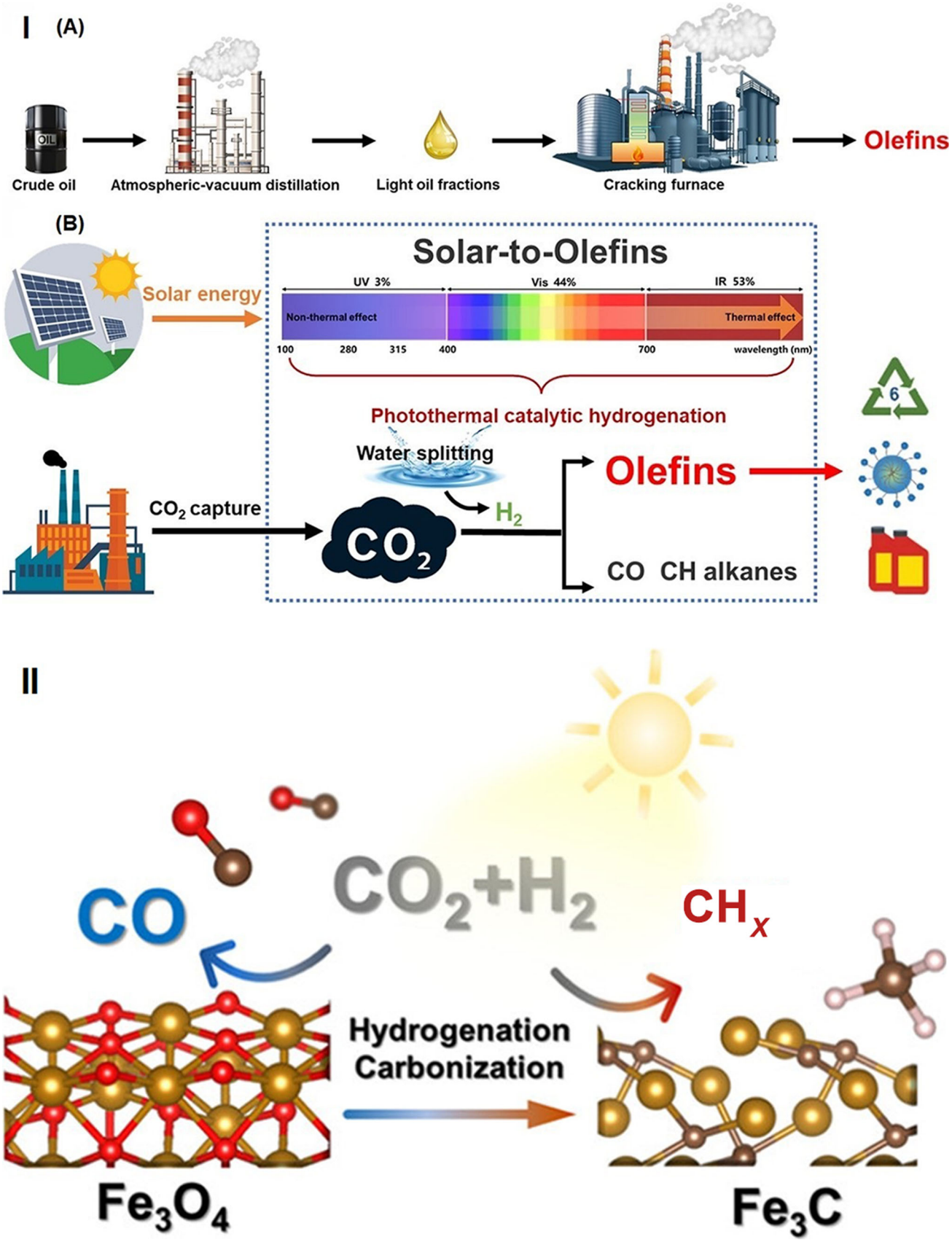

FIGURE 15 | Legend on next page.

$$CO_2 + H_2 \leftrightarrow CO + H_2O$$

At this stage, iron oxide species are reduced by hydrogen, producing water and creating OV on the catalyst surface. These defective FeO_x centers promote CO_2 adsorption and dissociation, resulting in CO* species formation. These intermediates can then evolve through three main pathways. Firstly, they can dissociate into atomic species with subsequent carbon migration to iron oxides, leading to their carburization—converting into carbides. Efficient carburization at the initial process time is one of the determinant factors in further hydrocarbon formation. Second, CO* species can desorb with gaseous CO byproduct formation. Finally, CO* intermediates can transfer to FTS active sites and participate in the further polymerization process. The FTS is the second main stage of CO_2 hydrogenation over Fe-based catalysts:

$$nCO + 2nH_2 \rightarrow C_nH_{2n} + nH_2O$$

$$nCO + (2n + 1)H_2 \rightarrow C_nH_{2n+2} + nH_2O$$

This stage primarily occurs on iron carbides, with Hägg iron carbide χ-Fe_5C_2 considered the most active. On these sites, numerous C-C coupling reactions occur alongside the hydrogenation of intermediates, resulting in a wide variety of hydrocarbons (both saturated and unsaturated) and oxygenated products. Several factors that determine the distribution of these products can be identified.

First, reaction kinetics restricts the proportion of each hydrocarbon fraction. This limitation can be expressed with sufficient accuracy by the Anderson-Schulz-Flory (ASF) distribution derived from the assumption that the rate of addition of a hydrocarbon unit does not depend on the current size of the growing chain [150]:

$$\chi_n = n(1 - \alpha)^2 \cdot \alpha^{n-1},$$

$$\alpha = \frac{r_1}{r_1 + r_2},$$

where χ_n is the weight fraction of C_n hydrocarbon products, α is the chain growth probability, n is the number of carbon atoms in a product molecule, r_1 is the chain propagation rate, and r_2 is the chain termination rate. A graphical representation of this distribution is shown in Figure 18.

As shown in Figure 18, only ~60% of C_2–C_4 products can be obtained in the hydrocarbon mixture via FTS. It is important to note that this value represents "CO-free selectivity", as the distribution excludes desorbed CO, which does not participate in the Fischer–Tropsch reaction. Furthermore, this percentage includes both light olefins and light paraffins selectivities. As a result, the main strategic goals are (1) increasing olefins fraction among the C_2–C_4 products and (2) decreasing CO selectivity.

The most common solution for the first issue is to modify the catalytic surface with alkali and alkaline earth metals. Acting as electronic promoters, these additives facilitate CO_2 adsorption while hindering H_2 adsorption. This increases the C/H ratio on the catalyst surface, thereby improving catalyst surface carburization, reducing methanation, promoting chain growth in Fischer–Tropsch synthesis, and reducing secondary hydrogenation of the resulting olefins. A detailed consideration of the effects of such electronic promoters is proposed in the corresponding chapter.

The second issue can be solved by enhancing the CO* involvement in hydrocarbon synthesis rather than allowing its desorption. This can be accomplished by structuring the active center, for example, by deliberately creating interfaces between iron oxide and iron carbide. Additionally, the structure and composition of the active site can be modified through catalyst promotion with a transition metal or by optimizing iron-support interactions. Such modifications may also activate alternative reaction pathways that could overcome ASF limitations. We discuss several corresponding examples in the chapters devoted to specific catalyst compositions.

9 | Cutting-Edge Catalysts and Future Prospects

To discuss recent trends in CO_2 hydrogenation into light olefins via the CO_2-FTS pathway, we prepared a scheme, demonstrating the performance of the best current catalysts reported (Figure 19). As can be seen, a wide range of Al_2O_3-, ZrO_2-, carbon-supported catalysts, as well as multifunctional catalysts, such as Fe-Co, Fe-Mn, and others, demonstrate both high light olefins yield and their space-time productivity. Among this diversity, the zeolite-functionalized iron catalysts achieve better percent olefins yield, while the supported Fe-Co catalysts demonstrate better STY values. Nevertheless, most of the discussed catalysts show comparable performance values (red circle).

At the same time, a few catalysts stand out clearly. Notably, three of these five compositions are well-structured carbon-supported iron catalysts. Two of these—the P-1.2 [106] and the 0.8Fe@0.28F-MC + 0.02K [39]—represent core-shell structures, comprising a FeO_x-FeC_x core with close proximity of active phases and a graphite or mesoporous carbon shell, preventing the core from sintering and chemical degradation. In turn, a

FIGURE 15 | (I) Schematic representation of light olefins production. (A) The conventional large-scale production process in the petrochemical industry. (B) A conceptual process diagram illustrating the solar-driven production of light olefins using abundant CO_2 and H_2O. This approach demonstrates a viable method for producing CO_2-derived light olefins under sunlight. H_2 is generated through light-driven water splitting. A crucial aspect of this process is the photodriven hydrogenation of CO_2 into light olefins, efficiently achieved using the photothermal catalytic method developed in this study with the K-Ru/Fe_3O_4 catalyst. The photothermal catalyst, powered by sunlight, produces light olefins with a high O/P ratio. Reproduced with permission: Copyright 2024, Elsevier [135]. (II) Photothermal conversion of CO_2 with tunable selectivity using Fe-based catalysts transition from oxides to carbides. Reproduced with permission: Copyright 2020, American Chemical Society [136].

GO/K-Fe-Co [112] catalyst was prepared via directed engineering of joint metal active phase utilizing the novel graphene fencing technique.

The best light olefins percent yield of about 30% was achieved over an R-FCK/SAPO [32] catalyst, which was represented with $Fe_{0.45}Cu_{0.45}K_{0.10}$ and SAPO-34 zeolite mechanical mixture. In this case, SAPO-34 not only improved the Fe-Cu-K dispersity but also promoted exposure of the active Cu-Fe(100) interface. Moreover, this mixed catalyst provides new pathways for CO* species hydrogenation, including the formation of additional HCOO* and *COOH intermediates, further enhancing light olefins selectivity. Finally, the MOF-prepared K-promoted trimetallic Fe-Co-Ni catalyst (FCN-K(a) [129]) also demonstrated both excellent light olefins yield and productivity. In this case, its performance was primarily attributed to developed porosity,

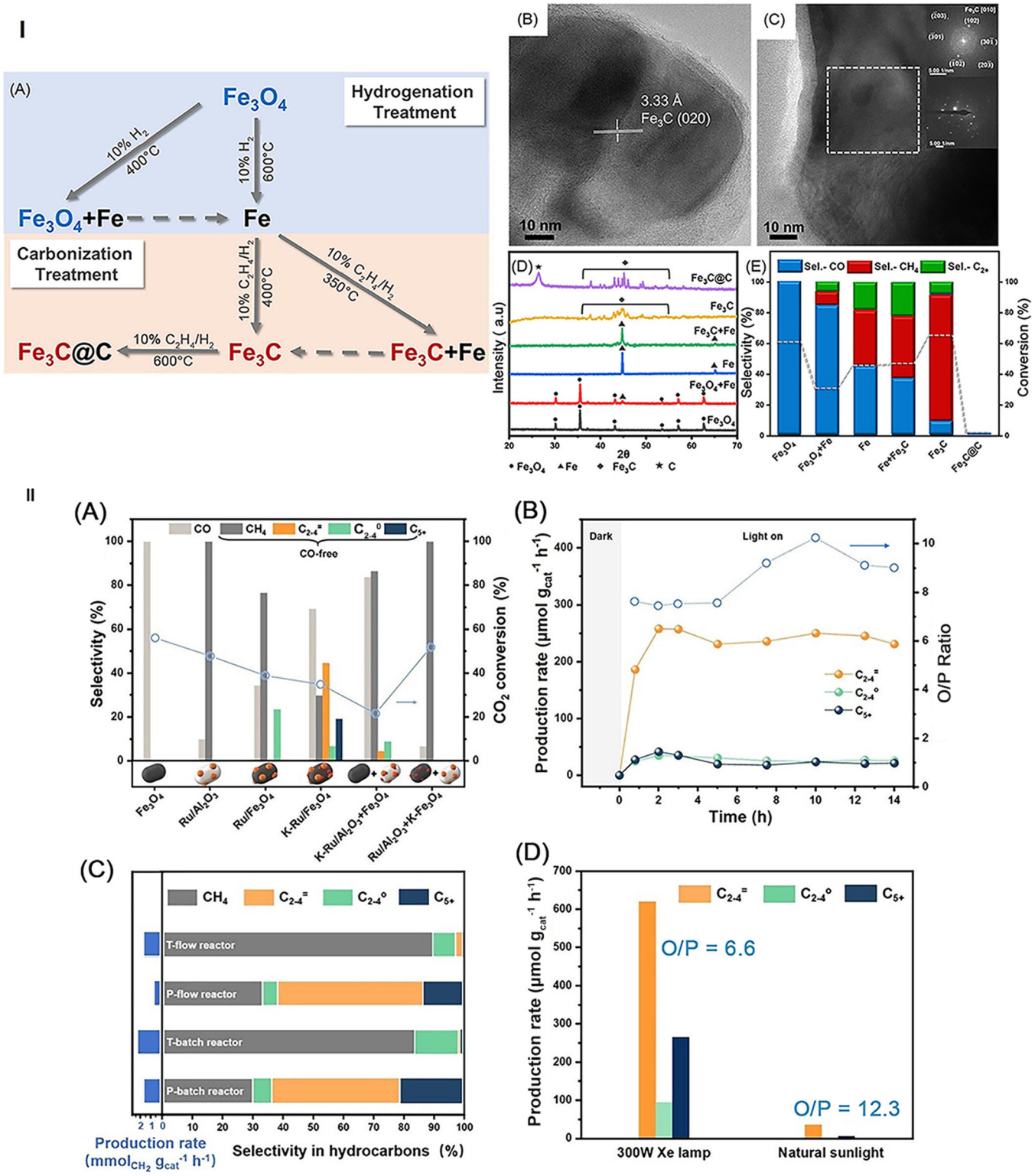

FIGURE 16 | Legend on next page.

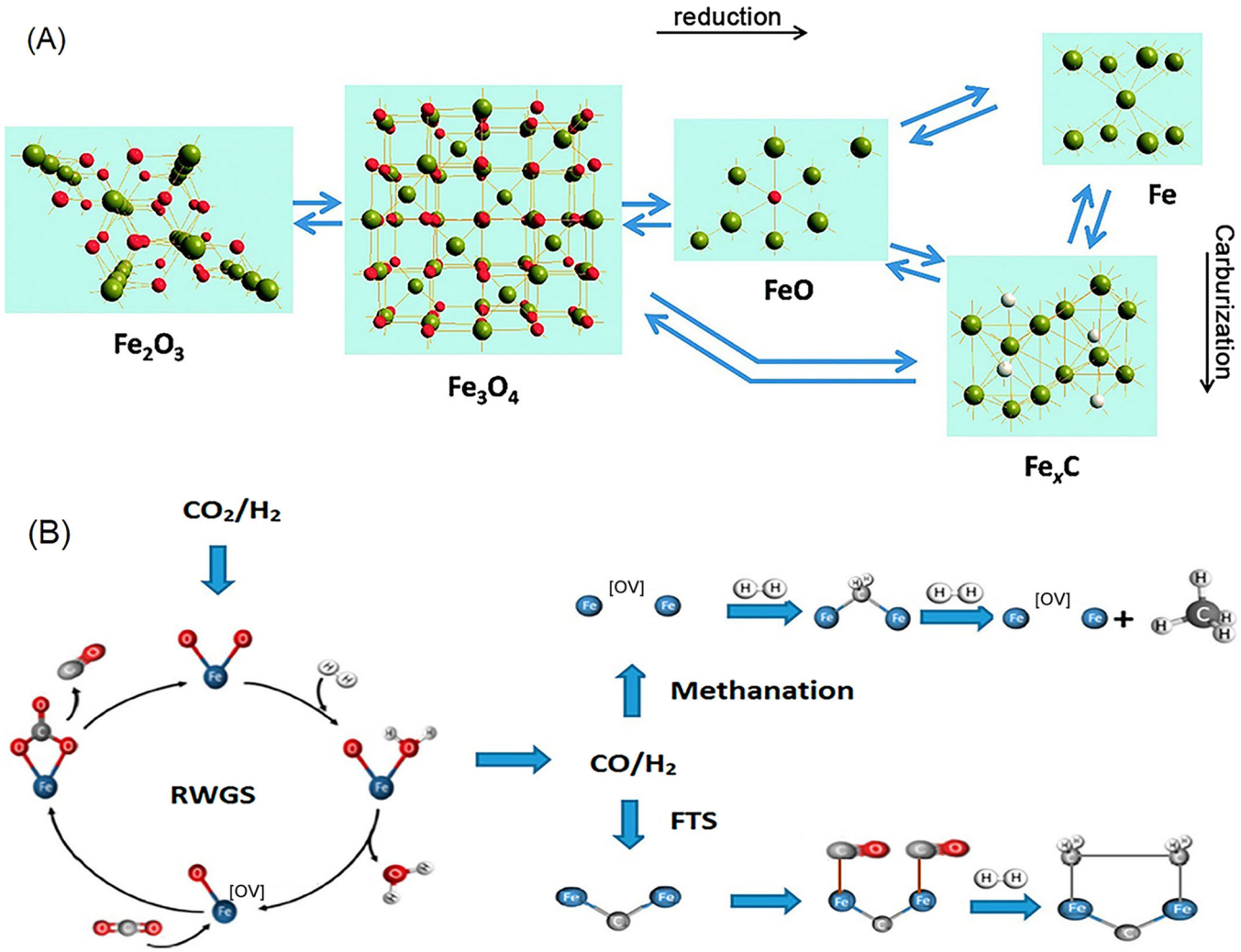

FIGURE 17 | (A) Iron phases transformations during catalytic CO_2 hydrogenation. Reproduced with permission: Copyright 2021, Royal Society of Chemistry [148]. (B) Schematic mechanism of CO_2-FTS process. Reproduced with permission: Copyright 2017, American Chemical Society [149].

an optimal Fe_3O_4/Fe_5C_2 ratio, and the effects of alkali metal promotion.

Therefore, beyond the most common Fe-catalyst design directions, such as improving catalyst dispersion, electronic promotion, and optimizing phase composition, the discussed edge studies propose two novel strategies. First, the directed engineering of the active center structure can be designated. Developing synthetic approaches with precise tailoring of the active center structure can bring principal advancement in the activity, stability, and selectivity of Fe-based catalysts by bringing he active phases proximity closer, generating new active interfaces, and steric protection of an active site. Another strategy is multifunctional tandem catalyst development. In this

FIGURE 16 | (I) (A) Preparation method for photothermal catalysts with varying levels of hydrogenation and carbonization. (B, C) Representative high-resolution transmission electron microscopy images of Fe_3C, with the inset showing the selective area electron diffraction of the highlighted white-framed region. (D) X-ray diffraction patterns of catalysts with different degrees of hydrogenation and carbonization. (E) Catalytic performance of photothermal CO_2 conversion using various Fe-based catalysts, where the dashed line represents CO_2 conversion (right axis) and the colored bars indicate product selectivity (left axis). Reaction conditions: 150 mg catalyst, xenon light, 2.05 W cm^{-2} light intensity, 4 h, $CO_2/H_2/Ar$ = 20:60:20. Reproduced with permission: Copyright 2020, American Chemical Society [136]. (II) Catalytic performances of various catalysts in the CO_2 hydrogenation reaction. (A) Photothermal catalytic performance of K-Ru/Fe_3O_4 and other control catalysts after 0.5 h of illumination in a batch reactor. (B) Continuous photothermal catalytic testing with the K-Ru/Fe_3O_4 catalyst. Reaction parameters: 80 mg catalyst, xenon light source, 2.05 W cm^{-2} light intensity, gas mixture $CO_2/H_2/Ar$ = 20:60:20, 2 mL min^{-1} flow rate, and 0.1 MPa pressure. (C) Comparison of hydrocarbon production rates and selectivity across different reactor types using the K-Ru/Fe_3O_4 catalyst under thermal (T) and photothermal (P) conditions. Thermal flow reaction conditions: 420°C, 2 mL min^{-1} flow rate. (D) Hydrocarbon production rate achieved with the K-Ru/Fe_3O_4 catalyst under xenon light and natural sunlight (with a Fresnel lens) in a batch reactor. Reproduced with permission: Copyright 2024, Elsevier [135].

regard, suitable zeolite (first of all, SAPO-34), being added to a Fe-based material, could not only regulate its CO_2-FTS activity but also serve as a co-catalytic component facilitating new reaction pathways in addition to the classical RWGS-FTS with a potential to overcome the Fischer–Tropsch kinetics limitations.

10 | Conclusions

This review provides a comprehensive overview of the current Fe-based thermocatalysts and photothermal catalysts for light olefins production via CO_2 hydrogenation. The low cost, high activity, and stability of iron-containing materials make them promising catalysts for efficient light olefins production. However, critical challenges remain in optimizing CO_2 activation, overcoming the Fischer–Tropsch kinetic limitations, and achieving high selectivity amid a broad product distribution.

The current literature demonstrates that electronic promoters can significantly improve catalyst performance by increasing the surface C/H ratio, which in turn enhances catalyst carburization, promotes C-C coupling, and reduces both methanation and secondary hydrogenation of the olefins formed. Moreover, the modification of Fe-based catalysts with transition metals—such as Zn, Mn, and Co—has been shown to enhance performance through the formation of joint phases and interfacial active surfaces. Iron-support interactions offer an additional approach to modifying catalyst properties. In this context, oxide (such as Al_2O_3 or ZrO_2) and carbon-based supports represent the most extensively studied options.

The development of tandem catalysts, including combinations of Fe-based materials with zeolites, presents another promising strategy by enabling alternative CO_2 conversion pathways that may overcome the intrinsic kinetic constraints of the Fischer–Tropsch synthesis. Finally, photothermal approaches further enhance both CO_2 conversion and light olefins selectivity by highly efficient solar energy utilization.

Collectively, these advancements underscore the potential of Fe-based catalysts in addressing challenges in CO_2 utilization. Future research aimed at fine-tuning catalyst composition, structure, and support interactions is expected to yield further improvements in activity, selectivity, and stability, ultimately advancing the sustainable production of light olefins.

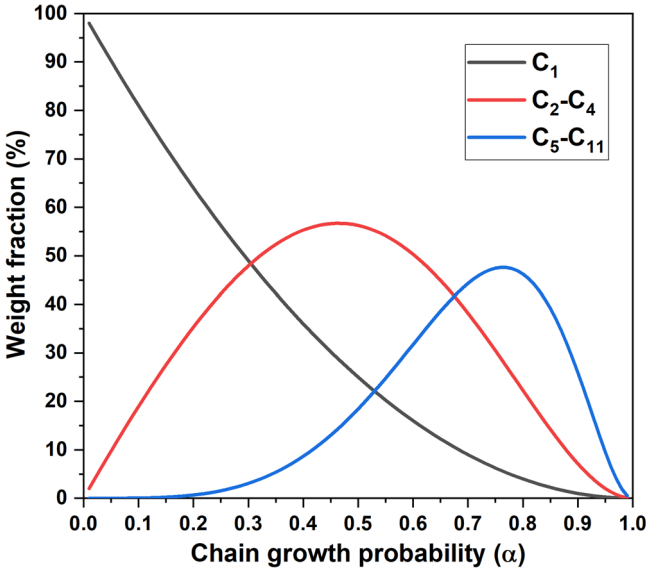

FIGURE 18 | Anderson–Schulz–Flory distribution for the Fischer–Tropsch synthesis.

Author Contributions

Timofey Karnaukhov: writing – original draft, investigation, data curation, methodology, formal analysis, visualization. **Blaž Likozar:** funding acquisition, supervision. **Andrii Kostyniuk:** writing – original draft, investigation, data curation, methodology, formal analysis, visualization.

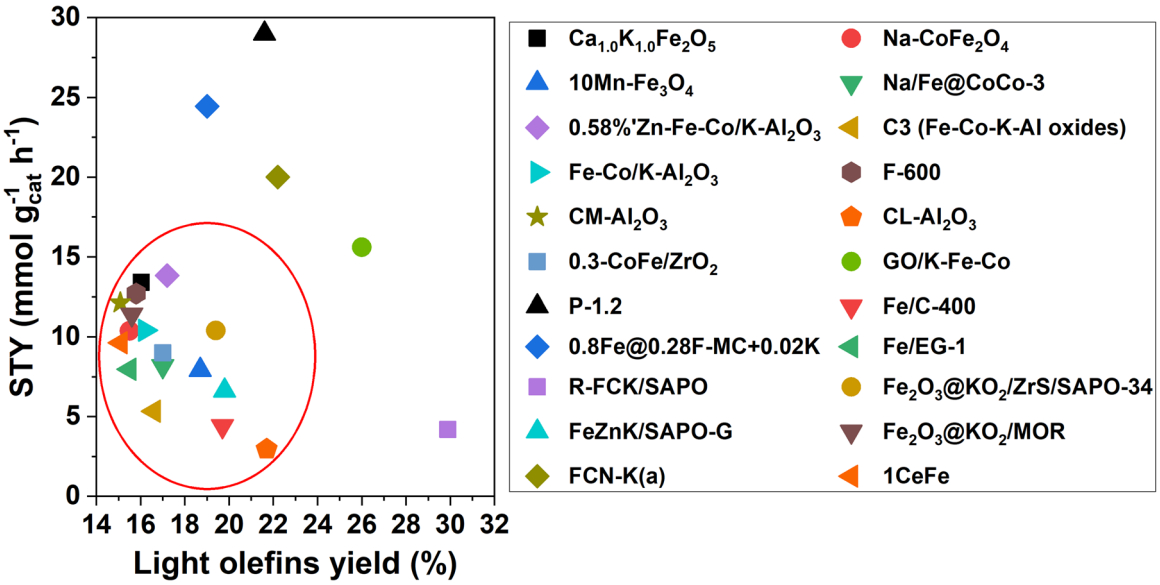

FIGURE 19 | The most efficient Fe-based catalysts of CO_2 conversion into light olefins.

Acknowledgments

The authors gratefully acknowledge the financial support provided under the doctoral program Scientists4Future Slovenia, funded by the Ministry of Higher Education, Science and Innovation, and the Slovenian Research Agency (ARIS) through research grants J7-4638 (Unlocking the Selective Catalytic Conversion Processes of CO_2 to Ethanol – UliSess) and J2-4441 (Dual-functional Nb_2O_5 and Nb_2O_5-TiO_2 materials for simultaneous CO_2 reduction and organic substance oxidation to value-added compounds).

Conflicts of Interest

The authors declare no conflicts of interest.

Data Availability Statement

Data will be made available on request.

References

1. F. Zeng, C. Mebrahtu, X. Xi, et al., "Catalysts Design for Higher Alcohols Synthesis by CO_2 Hydrogenation: Trends and Future Perspectives," *Applied Catalysis, B: Environmental* 291 (2021): 120073.

2. M. Ishizu, Y. Miyazawa, and X. Guo, "Long-Term Variations in Ocean Acidification Indices in the Northwest Pacific From 1993 to 2018," *Climatic Change* 168 (2021): 29.

3. M. Rubino, D. Etheridge, D. Thornton, et al., "Law Dome Ice Core 2000-Year CO_2, CH_4, N_2O and d13C-CO_2," v3. CSIRO. Data Collection (2019), https://doi.org/10.25919/5bfe29ff807fb.

4. F. Wang, J. D. Harindintwali, Z. Yuan, et al., "Technologies and Perspectives for Achieving Carbon Neutrality," *Innovation* 2, no. 4 (2021): 100180.

5. S. Chen, J. Liu, Q. Zhang, F. Teng, and B. C. McLellan, "A Critical Review on Deployment Planning and Risk Analysis of Carbon Capture, Utilization, and Storage (CCUS) Toward Carbon Neutrality," *Renewable and Sustainable Energy Reviews* 167 (2022): 112537.

6. L. Dou, L. Sun, W. Lyu, et al., "Trend of Global Carbon Dioxide Capture, Utilization and Storage Industry and Challenges and Countermeasures in China," *Petroleum Exploration and Development* 50, no. 5 (2023): 1246–1260.

7. B. Dziejarski, R. Krzyżyńska, and K. Andersson, "Current Status of Carbon Capture, Utilization, and Storage Technologies in the Global Economy: A Survey of Technical Assessment," *Fuel* 342 (2023): 127776.

8. W. Y. Hong, "A Techno-Economic Review on Carbon Capture, Utilisation and Storage Systems for Achieving a Net-Zero CO_2 Emissions Future," *Carbon Capture Science & Technology* 3 (2022): 100044.

9. R. Supriya, R. Chaudhury, U. Sharma, P. C. Thapliyal, and L. P. Singh, "Low-CO_2 Emission Strategies to Achieve Net Zero Target in Cement Sector," *Journal of Cleaner Production* 417 (2023): 137466.

10. P. Madejski, K. Chmiel, N. Subramanian, and T. Kuś, "Methods and Techniques for CO_2 Capture: Review of Potential Solutions and Applications in Modern Energy Technologies," *Energies* 15, no. 3 (2022): 887.

11. F. Wang, G. Wang, H. Wang, et al., "Analysis of the Current Status and Hot Technologies of Carbon Dioxide Geological Storage," *Processes* 12, no. 7 (2024): 1347.

12. W. Gao, S. Liang, R. Wang, et al., "Industrial Carbon Dioxide Capture and Utilization: State of the Art and Future Challenges," *Chemical Society Reviews* 49, no. 23 (2020): 8584–8686.

13. Z. Zhang, S. Y. Pan, H. Li, et al., "Recent Advances in Carbon Dioxide Utilization," *Renewable and Sustainable Energy Reviews* 125 (2020): 109799.

14. X. Zhang, W. Huang, L. Yu, et al., "Enabling Heterogeneous Catalysis to Achieve Carbon Neutrality: Directional Catalytic Conversion of CO_2 Into Carboxylic Acids," *Carbon Energy* 6, no. 3 (2024): e362.

15. A. D. N. Kamkeng, M. Wang, J. Hu, W. Du, and F. Qian, "Transformation Technologies for CO_2 Utilisation: Current Status, Challenges and Future Prospects," *Chemical Engineering Journal* 409 (2021): 128138.

16. L. Wang, D. Wang, and Y. Li, "Single-Atom Catalysis for Carbon Neutrality," *Carbon Energy* 4, no. 6 (2022): 1021–1079.

17. A. Kostyniuk and B. Likozar, "State-of-the-Art Advancements in the Thermocatalytic Conversion of CO_2 Into Ethanol and Higher Alcohols: Recent Progress in Catalyst Development and Reaction Mechanisms," *Chemical Engineering Journal* 503 (2025): 158467.

18. Q. Yang, Y. Fan, D. Rong, R. Bao, and D. Zhang, "An Auto-Configurable Machine Learning Framework to Optimize and Predict Catalysts for CO_2 to Light Olefins Process," *AIChE Journal* 70, no. 8 (2024): e18437.

19. S. A. Chernyak, M. Corda, J. P. Dath, V. V. Ordomsky, and A. Y. Khodakov, "Light Olefin Synthesis From a Diversity of Renewable and Fossil Feedstocks: State-of-the-Art and Outlook," *Chemical Society Reviews* 51, no. 18 (2022): 7994–8044.

20. Q. W. Song, R. Ma, P. Liu, K. Zhang, and L. N. He, "Recent Progress in CO_2 Conversion Into Organic Chemicals by Molecular Catalysis," *Green Chemistry* 25, no. 17 (2023): 6538–6560.

21. S. De, A. Dokania, A. Ramirez, and J. Gascon, "Advances in the Design of Heterogeneous Catalysts and Thermocatalytic Processes for CO_2 Utilization," *ACS Catalysis* 10, no. 23 (2020): 14147–14185.

22. K. Sun, Y. Qian, and H. L. Jiang, "Metal-Organic Frameworks for Photocatalytic Water Splitting and CO_2 Reduction," *Angewandte Chemie International Edition* 62, no. 15 (2023): e202217565.

23. L. P. Thulluru, M. M. Ghangrekar, and S. Chowdhury, "Progress and Perspectives on Microbial Electrosynthesis for Valorisation of CO_2 Into Value-Added Products," *Journal of Environmental Management* 332 (2023): 117323.

24. B. Chang, H. Pang, F. Raziq, et al., "Electrochemical Reduction of Carbon Dioxide to Multicarbon (C_{2+}) Products: Challenges and Perspectives," *Energy & Environmental Science* 16, no. 11 (2023): 4714–4758.

25. D. Xu, K. Li, B. Jia, et al., "Electrocatalytic CO_2 Reduction Towards Industrial Applications," *Carbon Energy* 5, no. 1 (2023): e230.

26. A. Modak, P. Bhanja, S. Dutta, B. Chowdhury, and A. Bhaumik, "Catalytic Reduction of CO_2 Into Fuels and Fine Chemicals," *Green Chemistry* 22, no. 13 (2020): 4002–4033.

27. J. Chen, X. Zhao, M. Shakouri, and H. Wang, "A Specific Review of CO_2 Catalytic Conversion Reactions Based on the Concept of Catalytic Sites Contiguity," *ChemCatChem* 16, no. 22 (2024): e202400287.

28. J. Y. Jia, Y. L. Shan, Y. X. Tuo, H. Yan, X. Feng, and D. Chen, "Review of Iron-Based Catalysts for Carbon Dioxide Fischer–Tropsch Synthesis," *Transactions of Tianjin University* 30, no. 2 (2024): 178–197.

29. H. Tang, T. Qiu, X. Wang, C. Zhang, and Z. Zhang, "A Brief Review of Recent Theoretical Advances in Fe-Based Catalysts for CO_2 Hydrogenation," *Molecules* 29, no. 6 (2024): 1194.

30. P. Zhang, F. Han, J. Yan, X. Qiao, Q. Guan, and W. Li, "N-Doped Ordered Mesoporous Carbon (N-OMC) Confined Fe_3O_4-FeC_x Heterojunction for Efficient Conversion of CO_2 to Light Olefins," *Applied Catalysis, B: Environmental* 299 (2021): 120639.

31. G. Singh, D. Khurana, T. S. Khan, et al., "Insight Into Mn Enhanced Short-Chain Olefins Selectivity in CO_2 Hydrogenation Over Na-$CuFeO_2$ Catalyst," *Applied Surface Science* 616 (2023): 156401.

32. J. Ding, Q. Liu, R. Ye, et al., "Metal–Support Interactions in Fe–Cu–K Admixed With SAPO-34 Catalysts for Highly Selective Transformation of CO_2 and H_2 Into Lower Olefins," *Journal of Materials Chemistry A* 9, no. 38 (2021): 21877–21887.

33. Q. Liu, J. Ding, R. Wang, and Q. Zhong, "FeZnK/SAPO-34 Catalyst for Efficient Conversion of CO_2 to Light Olefins," *Catalysis Letters* 153, no. 1 (2023): 54–61.

34. H. Zhao, L. Guo, W. Gao, et al., "Multi-Promoters Regulated Iron Catalyst With Well-Matching Reverse Water-Gas Shift and Chain Propagation for Boosting CO_2 Hydrogenation," *Journal of CO2 Utilization* 52 (2021): 101700.

35. Q. Zhao, X. Xu, G. Fan, and F. Li, "Crucial Role of Surface FeO_x Components on Supported Fe-Based Nanocatalysts for CO_2 Hydrogenation to Light Olefins," *Industrial & Engineering Chemistry Research* 62, no. 24 (2023): 9420–9432.

36. T. Witoon, N. Chaipraditgul, T. Numpilai, et al., "Highly Active Fe-Co-Zn/K-Al_2O_3 Catalysts for CO_2 Hydrogenation to Light Olefins," *Chemical Engineering Science* 233 (2021): 116428.

37. P. Zhang, J. Yan, F. Han, X. Qiao, Q. Guan, and W. Li, "Controllable Assembly of Fe_3O_4-Fe_3C@MC by In Situ Doping of Mn for CO_2 Selective Hydrogenation to Light Olefins," *Catalysis Science & Technology* 12, no. 7 (2022): 2360–2368.

38. K. Jin, C. Wen, L. Chen, et al., "In Situ Synthesis of Highly Dispersed Fe/C Catalysts With Pomelo Peel as Carbon Source in CO_2 Hydrogenation to Light Olefins," *Fuel* 333 (2023): 126412.

39. P. Zhang, F. Han, J. Yan, et al., "Heteroatom Induced Synthesis of FeO-Fe_3C Confined Within F-Doped Graphene Shell for Efficient CO_2 Hydrogenation to Light Olefins," *Chemical Engineering Journal* 477 (2023): 147153.

40. A. V. P. Lino, E. M. Assaf, and J. M. Assaf, "Production of Light Hydrocarbons at Atmospheric Pressure From CO_2 Hydrogenation Using $Ce_xZr_{(1-X)}O_2$ Iron-Based Catalysts," *Journal of CO2 Utilization* 55 (2022): 101805.

41. A. V. Paladino Lino, L. H. Vieira, E. M. Assaf, and J. M. Assaf, "Effects of the Potassium Incorporation in Fe–Ce–Zr Based Catalysts and Activation Condition in CO_2 Hydrogenation to C_2/C_3 Olefins at Atmospheric Pressure," *International Journal of Hydrogen Energy* 51, no. B (2024): 1122–1140.

42. B. A. Oni, S. E. Sanni, and A. J. Ibegbu, "Production of Light Olefins by Catalytic Hydrogenation of CO_2 Over Y_2O_3/Fe-Co Modified With SAPO-34," *Applied Catalysis, A: General* 643 (2022): 118784.

43. Z. Zhang, H. Yin, G. Yu, et al., "Selective Hydrogenation of CO_2 and CO Into Olefins Over Sodium- and Zinc-Promoted Iron Carbide Catalysts," *Journal of Catalysis* 395 (2021): 350–361.

44. C. Dai, X. Zhao, B. Hu, et al., "Effect of EDTA-2Na Modification on Fe-Co/Al_2O_3 for Hydrogenation of Carbon Dioxide to Lower Olefins and Gasoline," *Journal of CO2 Utilization* 43 (2021): 101369.

45. J. Jiang, C. Wen, Z. Tian, et al., "Manganese-Promoted Fe_3O_4 Microsphere for Efficient Conversion of CO_2 to Light Olefins," *Industrial & Engineering Chemistry Research* 59, no. 5 (2020): 2155–2162.

46. M. Albrecht, U. Rodemerck, M. Schneider, M. Bröring, D. Baabe, and E. V. Kondratenko, "Unexpectedly Efficient CO_2 Hydrogenation to Higher Hydrocarbons over Non-Doped Fe_2O_3," *Applied Catalysis, B: Environmental* 204 (2017): 119–126.

47. H. Zhao, C. Zeng, and N. Tsubaki, "A Mini Review on Recent Advances in Thermocatalytic Hydrogenation of Carbon Dioxide to Value-Added Chemicals and Fuels," *Resources Chemicals and Materials* 1, no. 3–4 (2022): 230–248.

48. F. Jiang, B. Liu, S. Geng, Y. Xu, and X. Liu, "Hydrogenation of CO_2 Into Hydrocarbons: Enhanced Catalytic Activity Over Fe-Based Fischer–Tropsch Catalysts," *Catalysis Science & Technology* 8, no. 16 (2018): 4097–4107.

49. J. Wei, J. Sun, Z. Wen, C. Fang, Q. Ge, and H. Xu, "New Insights Into the Effect of Sodium on Fe_3O_4-Based Nanocatalysts for CO_2 Hydrogenation to Light Olefins," *Catalysis Science & Technology* 6, no. 13 (2016): 4786–4793.

50. C. Wei, W. Tu, L. Jia, et al., "The Evolutions of Carbon and Iron Species Modified by Na and Their Tuning Effect on the Hydrogenation of CO_2 to Olefins," *Applied Surface Science* 525 (2020): 146622.

51. H. S. Malhi, C. Sun, Z. Zhang, et al., "Catalytic Consequences of the Decoration of Sodium and Zinc Atoms During CO_2 Hydrogenation to Olefins Over Iron-Based Catalyst," *Catalysis Today* 387 (2022): 28–37.

52. F. Yuan, G. Zhang, J. Zhu, et al., "Boosting Light Olefin Selectivity in CO_2 Hydrogenation by Adding Co to Fe Catalysts Within Close Proximity," *Catalysis Today* 371 (2021): 142–149.

53. J. Zhu, M. Mu, Y. Liu, et al., "Unveiling the Promoting Effect of Potassium on the Structural Evolution of Iron Catalysts During CO_2 Hydrogenation," *Chemical Engineering Science* 282 (2023): 119228.

54. A. Russkikh, G. Shterk, B. H. Al-Solami, B. A. Fadhel, A. Ramirez, and J. Gascon, "Turning Waste Into Value: Potassium-Promoted Red Mud as an Effective Catalyst for the Hydrogenation of CO_2," *Chemsuschem* 13, no. 11 (2020): 2981–2987.

55. Z. Sun, X. Chen, F. Lu, L. Zhou, and Y. Zhang, "Effect of Rb Promoter on Fe_3O_4 Microsphere Catalyst for CO_2 Hydrogenation to Light Olefins," *Catalysis Communications* 162 (2022): 106387.

56. Y. Zhou, A. Sadia Traore, D. V. Peron, et al., "Promotion Effects of Alkali Metals on Iron Molybdate Catalysts for CO_2 Catalytic Hydrogenation," *Journal of Energy Chemistry* 85 (2023): 291–300.

57. A. J. Barrios, D. V. Peron, A. Chakkingal, et al., "Efficient Promoters and Reaction Paths in the CO_2 Hydrogenation to Light Olefins Over Zirconia-Supported Iron Catalysts," *ACS Catalysis* 12, no. 5 (2022): 3211–3225.

58. K. Liu, D. Xu, H. Fan, et al., "Development of Mg-Modified Fe-Based Catalysts for Low-Concentration CO_2 Hydrogenation to Olefins," *ACS Sustainable Chemistry & Engineering* 12, no. 5 (2024): 2070–2079.

59. J. I. Orege, J. Wei, Y. Han, et al., "Highly Stable Sr and Na co-Decorated Fe Catalyst for High-Valued Olefin Synthesis From CO_2 Hydrogenation," *Applied Catalysis, B: Environmental* 316 (2022): 121640.

60. J. I. Orege, N. Liu, C. C. Amoo, J. Wei, Q. Ge, and J. Sun, "Boosting CO_2 Hydrogenation to High-Value Olefins With Highly Stable Performance Over Ba and Na co-Modified Fe Catalyst," *Journal of Energy Chemistry* 80 (2023): 614–624.

61. A. Cui, M. Wu, T. Guo, X. Sun, Y. Chen, and Q. Guo, "Potassium-Modified Calcium-Ferrate-Catalyzed Hydrogenation of Carbon Dioxide to Produce Light Olefins," *New Journal of Chemistry* 48, no. 28 (2024): 12616–12625.

62. H. Chen, N. Ma, C. Wang, et al., "Mechanochemical Incorporation of Magnesium in Iron-Based Composite Surface for Efficient Hydrogenation of Carbon Dioxide to Light Olefin," *Fuel* 331, no. 1 (2023): 125849.

63. H. Yang, Y. Dang, X. Cui, et al., "Selective Synthesis of Olefins via CO_2 Hydrogenation Over Transition-Metal-Doped Iron-Based Catalysts," *Applied Catalysis, B: Environmental* 321 (2023): 122050.

64. X. Liu, M. Xu, C. Cao, Z. Yang, and J. Xu, "Effects of Zinc on χ-Fe_5C_2 for Carbon Dioxide Hydrogenation to Olefins: Insights From Experimental and Density Function Theory Calculations," *Chinese Journal of Chemical Engineering* 54 (2023): 206–214.

65. Q. Yang, R. Wang, X. Zhang, et al., "Topotactic Transformation of Metal–Organic Frameworks to Iron-Based Catalysts for the Direct Hydrogenation of CO_2 to Olefins," *Catalysis Science & Technology* 13, no. 11 (2023): 3258–3269.

66. L. Guo, J. Li, Y. Zeng, et al., "Heteroatom Doped Iron-Based Catalysts Prepared by Urea Self-Combustion Method for Efficient CO_2 Hydrogenation," *Fuel* 276 (2020): 118102.

67. X. Wang, J. Zhang, J. Chen, Q. Ma, S. Fan, and T. Zhao, "Effect of Preparation Methods on the Structure and Catalytic Performance of Fe-Zn/K Catalysts for CO_2 Hydrogenation to Light Olefins," *Chinese Journal of Chemical Engineering* 26, no. 4 (2018): 761–767.

68. J. Zhang, S. Lu, X. Su, S. Fan, Q. Ma, and T. Zhao, "Selective Formation of Light Olefins From CO_2 Hydrogenation Over Fe-Zn-K Catalysts," *Journal of CO2 Utilization* 12 (2015): 95–100.

69. Y. Li, J. Chen, Z. Li, et al., "Selective Production of Light α-Olefins and Long-Chain α-Olefins From CO_2/H_2 and CO/H_2 Over Iron-Based Catalysts: Effects of Na_2S and H_2O," *Journal of Catalysis* 436 (2024): 115587.

70. Z. Zhang, C. Wei, L. Jia, et al., "Insights Into the Regulation of FeNa Catalysts Modified by Mn Promoter and Their Tuning Effect on the Hydrogenation of CO_2 to Light Olefins," *Journal of Catalysis* 390 (2020): 12–22.

71. M. Al-Dossary, A. A. Ismail, J. L. G. Fierro, H. Bouzid, and S. A. Al-Sayari, "Effect of Mn Loading Onto MnFeO Nanocomposites for the CO_2 Hydrogenation Reaction," *Applied Catalysis, B: Environmental* 165 (2015): 651–660.

72. B. Liu, S. Geng, J. Zheng, X. Jia, F. Jiang, and X. Liu, "Unravelling the New Roles of Na and Mn Promoter in CO_2 Hydrogenation Over Fe_3O_4-Based Catalysts for Enhanced Selectivity to Light A-Olefins," *ChemCatChem* 10, no. 20 (2018): 4718–4732.

73. Y. Xu, P. Zhai, Y. Deng, et al., "Highly Selective Olefin Production From CO_2 Hydrogenation on Iron Catalysts: A Subtle Synergy Between Manganese and Sodium Additives," *Angewandte Chemie International Edition* 59, no. 48 (2020): 21736–21744.

74. N. Liu, J. Wei, J. Xu, et al., "Elucidating the Structural Evolution of Highly Efficient Co–Fe Bimetallic Catalysts for the Hydrogenation of CO_2 Into Olefins," *Applied Catalysis, B: Environmental* 328 (2023): 122476.

75. Q. Xu, X. Xu, G. Fan, L. Yang, and F. Li, "Unveiling the Roles of Fe-Co Interactions Over Ternary Spinel-Type $ZnCo_XFe_{2-X}O_4$ Catalysts for Highly Efficient CO_2 Hydrogenation to Produce Light Olefins," *Journal of Catalysis* 400 (2021): 355–366.

76. H. Chen, C. Wang, M. Zheng, et al., "Reactive Ball-Milling Synthesis of Co-Fe Bimetallic Catalyst for Efficient Hydrogenation of Carbon Dioxide to Value-Added Hydrocarbons," *Journal of Energy Chemistry* 84 (2023): 210–218.

77. Y. Li, Y. He, K. Fujihara, et al., "A Core-Shell Structured Na/Fe@Co Bimetallic Catalyst for Light-Hydrocarbon Synthesis From CO_2 Hydrogenation," *Catalysts* 13, no. 7 (2023): 1090.

78. N. Dolsiririttigul, T. Numpilai, K. Faungnawakij, M. Chareonpanich, G. Rupprechter, and T. Witoon, "Exploring the Impact of Cobalt and H_2 to CO Ratios on Catalytic Performance of FeKAl and FeCoKAl Catalysts in CO Hydrogenation to Light Olefins," *Fuel* 383 (2025): 133833.

79. Y. Liu, B. Chen, R. Liu, et al., "CO_2 Hydrogenation to Olefins on Supported Iron Catalysts: Effects of Support Properties on Carbon-Containing Species and Product Distribution," *Fuel* 324, no. B (2022): 124649.

80. J. Bao, X. Xu, Q. Zhao, G. Fan, and F. Li, "Key Role of Metal Oxide Support in Tuning Active Surface Components of Fe-Based Catalysts for CO_2 Hydrogenation," *Energy & Fuels* 37, no. 20 (2023): 15943–15955.

81. N. Dolsiririttigul, T. Numpilai, K. Faungnawakij, M. Chareonpanich, G. Rupprechter, and T. Witoon, "Unraveling the Complex Interactions Between Structural Features and Reactivity of Iron-Based Catalysts Across Various Supports in the Synthesis of Light Olefins From Syngas," *Chemical Engineering Journal* 480 (2024): 148196.

82. J. Liu, A. Zhang, X. Jiang, et al., "Direct Transformation of Carbon Dioxide to Value-Added Hydrocarbons by Physical Mixtures of Fe_5C_2 and K-Modified Al_2O_3," *Industrial & Engineering Chemistry Research* 57, no. 28 (2018): 9120–9126.

83. T. Numpilai, T. Witoon, N. Chanlek, et al., "Structure–Activity Relationships of Fe-Co/K-Al_2O_3 Catalysts Calcined at Different Temperatures for CO_2 Hydrogenation to Light Olefins," *Applied Catalysis, A: General* 547 (2017): 219–229.

84. T. Numpilai, N. Chanlek, Y. Poo-Arporn, et al., "Pore Size Effects on Physicochemical Properties of Fe-Co/K-Al_2O_3 Catalysts and Their Catalytic Activity in CO_2 Hydrogenation to Light Olefins," *Applied Surface Science* 483 (2019): 581–592.

85. N. Chaipraditgul, T. Numpilai, C. Kui Cheng, et al., "Tuning Interaction of Surface-Adsorbed Species Over Fe/K-Al_2O_3 Modified With Transition Metals (Cu, Mn, V, Zn or Co) on Light Olefins Production From CO_2 Hydrogenation," *Fuel* 283 (2021): 119248.

86. T. Witoon, V. Lapkeatseree, T. Numpilai, C. Kui Cheng, and J. Limtrakul, "CO_2 Hydrogenation to Light Olefins Over Mixed Fe-Co-K-Al Oxides Catalysts Prepared via Precipitation and Reduction Methods," *Chemical Engineering Journal* 428 (2022): 131389.

87. N. Polsomboon, T. Numpilai, K. Jitapunkul, et al., "CO_2 Hydrogenation to Light Olefins over Fe–Co/K–Al_2O_3 Catalysts Prepared via Microwave Calcination," *Reaction Chemistry & Engineering* 10, no. 3 (2025): 515–533.

88. E. S. Borovinskaya, S. Oswald, and W. Reschetilowski, "Effects of Promoter on Structural and Surface Properties of Zirconium Oxide-Based Catalyst Materials," *Molecules* 25, no. 11 (2020): 2619.

89. P. Zhang, W. Na, J. Zuo, et al., "CO_2 Hydrogenation to Methanol Over Hydrothermally Synthesized In_x-Zr_y Catalysts," *Molecular Catalysis* 538 (2023): 112977.

90. H. Gu, J. Ding, Q. Zhong, Y. Zeng, and F. Song, "Promotion of Surface Oxygen Vacancies on the Light Olefins Synthesis From Catalytic CO_2 Hydrogenation Over Fe–K/ZrO_2 Catalysts," *International Journal of Hydrogen Energy* 44, no. 23 (2019): 11808–11816.

91. J. Ding, L. Huang, W. Gong, et al., "CO_2 Hydrogenation to Light Olefins With High-Performance $Fe_{0.30}Co_{0.15}Zr_{0.45}K_{0.10}O_{1.63}$," *Journal of Catalysis* 377 (2019): 224–232.

92. J. Ding, W. Zhao, L. Zi, et al., "Promotional Effect of ZrO_2 on Supported FeCoK Catalysts for Ethylene Synthesis From Catalytic CO_2 Hydrogenation," *International Journal of Hydrogen Energy* 45, no. 30 (2020): 15254–15262.

93. Q. Zhao, G. Fan, and F. Li, "Unique CuO –FeO Interfaces in Cu-Decorated Fe-Based Catalysts Facilitating CO_2 Hydrogenation to Higher Hydrocarbons," *Chemical Engineering Journal* 495 (2024): 153309.

94. J. Huang, S. Jiang, M. Wang, X. Wang, J. Gao, and C. Song, "Dynamic Evolution of Fe and Carbon Species Over Different ZrO_2 Supports During CO Prereduction and Their Effects on CO_2 Hydrogenation to Light Olefins," *ACS Sustainable Chemistry & Engineering* 9, no. 23 (2021): 7891–7903.

95. F. Xu, X. Meng, R. Zhao, et al., "Fe_2O_3@ZrO_2 Catalyst Derived From MOF-on-MOF for Direct CO_2 Hydrogenation to Light Olefins," *Chemical Engineering Journal* 494 (2024): 152926.

96. W. Li, A. Zhang, X. Jiang, et al., "The Anti-Sintering Catalysts: Fe–Co–Zr Polymetallic Fibers for CO_2 Hydrogenation to C_2= –C_4= –Rich Hydrocarbons," *Journal of CO2 Utilization* 23 (2018): 219–225.

97. J. Zhang, X. Su, X. Wang, Q. Ma, S. Fan, and T. S. Zhao, "Promotion Effects of Ce Added Fe–Zr–K on CO_2 Hydrogenation to Light Olefins," *Reaction Kinetics, Mechanisms and Catalysis* 124, no. 2 (2018): 575–585.

98. S. M. Schimming, G. S. Foo, O. D. LaMont, et al., "Kinetics of Hydrogen Activation on Ceria–Zirconia," *Journal of Catalysis* 329 (2015): 335–347.

99. J. Deng, S. Li, L. Xiong, J. Wang, S. Yuan, and Y. Chen, "Different Thermal Behavior of Nanostructured CeO_2-ZrO_2 Based Oxides With Varied Ce/Zr Molar Ratios," *Materials Chemistry and Physics* 236 (2019): 121767.

100. H. M. Torres Galvis, J. H. Bitter, C. B. Khare, M. Ruitenbeek, A. I. Dugulan, and K. P. de Jong, "Supported Iron Nanoparticles as Catalysts for Sustainable Production of Lower Olefins," *Science* 335, no. 6070 (2012): 835–838.

101. T. Witoon, T. Numpilai, K. Nueangnoraj, C. K. Cheng, M. Chareonpanich, and J. Limtrakul, "Light Olefins Synthesis From CO_2 Hydrogenation Over Mixed Fe–Co–K Supported on Micro-Mesoporous Carbon Catalysts," *International Journal of Hydrogen Energy* 47, no. 100 (2022): 42185–42199.

102. R. Zhao, X. Meng, W. Dai, et al., "Highly Dispersed Fe/EG Catalysts Assisted by Ammonium Citrate and Their Application in CO_2 Hydrogenation to Olefins," *Fuel* 351 (2023): 128926.

103. K. Y. Kim, H. Lee, W. Y. Noh, et al., "Cobalt Ferrite Nanoparticles to Form a Catalytic Co–Fe Alloy Carbide Phase for Selective CO_2 Hydrogenation to Light Olefins," *ACS Catalysis* 10, no. 15 (2020): 8660–8671.

104. B. Y. Chen, G. Dobele, A. Plavniece, et al., "Catalytic Hydrogenation of CO_2 to Light Olefins by Using K-Doped FeC_x Catalysts Derived From the Fe-Chitosan Complex," *International Journal of Hydrogen Energy* 48, no. 11 (2023): 4276–4286.

105. Y. Fu, C. C. Amoo, H. Qi, et al., "Edta Chemical Directly Orient CO_2 Hydrogenation Towards Olefins," *Chemical Engineering Journal* 438 (2022): 135597.

106. Z. Luo, F. Han, P. Zhang, et al., "The Construction of Iron-Based Catalysts Encapsulated by Graphite for CO_2 Hydrogenation to Light Olefins," *Chemical Engineering Journal* 490 (2024): 151674.

107. H. Qi, W. Si, Z. Xu, et al., "Facile Synthesis of Iron Carbide via Pyrolysis of Ferrous Fumarate for Catalytic CO_2 Hydrogenation to Lower Olefins," *Chemsuschem* 17, no. 16 (2024): e202400484.

108. Z. Dong, J. Zhao, Y. Tian, B. Zhang, and Y. Wu, "Preparation and Performances of ZIF-67-Derived FeCo Bimetallic Catalysts for CO_2 Hydrogenation to Light Olefins," *Catalysts* 10, no. 4 (2020): 455.

109. F. Xu, X. Meng, R. Zhao, et al., "Metal-Organic Framework-Derived Fe_3O_4-FeC_x Catalyst for Direct CO_2 Hydrogenation to Light Olefins," *Applied Catalysis, A: General* 670 (2024): 119537.

110. C. Chen, G. Song, Z. Wang, et al., "Insight Into the Synergistic Effect of Copper and Sodium Over Metal Organic Framework-Derived Fe-Based Catalyst for CO_2 Hydrogenation to Aromatics," *Applied Catalysis, B: Environmental* 341 (2024): 123330.

111. H. Pitayachinchot, P. Reubroycharoen, P. Prasassarakich, and C. Ngamcharussrivichai, "Highly Selective Iron-Based Catalysts Derived From Al-Containing MIL-53 for CO_2 Hydrogenation to Light Olefins," *Journal of Environmental Chemical Engineering* 12, no. 2 (2024): 112061.

112. J. Liang, J. Liu, L. Guo, et al., "CO_2 Hydrogenation Over Fe-Co Bimetallic Catalysts With Tunable Selectivity Through a Graphene Fencing Approach," *Nature Communications* 15, no. 1 (2024): 512.

113. X. Yang, R. Wang, J. Yang, et al., "Exploring the Reaction Paths in the Consecutive Fe-Based FT Catalyst–Zeolite Process for Syngas Conversion," *ACS Catalysis* 10, no. 6 (2020): 3797–3806.

114. T. Numpilai, S. Kahadit, T. Witoon, et al., "CO_2 Hydrogenation to Light Olefins Over In_2O_3/SAPO-34 and Fe-Co/K-Al_2O_3 Composite Catalyst," *Topics in Catalysis* 64, no. 5 (2021): 316–327.

115. A. Ramirez, A. Dutta Chowdhury, A. Dokania, et al., "Effect of Zeolite Topology and Reactor Configuration on the Direct Conversion of CO_2 to Light Olefins and Aromatics," *ACS Catalysis* 9, no. 7 (2019): 6320–6334.

116. A. Dokania, A. Dutta Chowdhury, A. Ramirez, et al., "Acidity Modification of ZSM-5 for Enhanced Production of Light Olefins From CO_2," *Journal of Catalysis* 381 (2020): 347–354.

117. A. Ramirez, A. Dutta Chowdhury, M. Caglayan, et al., "Coated Sulfated Zirconia/SAPO-34 for the Direct Conversion of CO_2 to Light Olefins," *Catalysis Science & Technology* 10, no. 5 (2020): 1507–1517.

118. Z. Cai, F. Zhang, X. Cao, et al., "The Effect of Mn, Al Doping on the CO_2 Hydrogenation Performance of $CaCO_3$-Supported Fe-Based Catalysts," *ChemPlusChem* 88, no. 8 (2023): e202300286.

119. L. Ma, X. Gao, J. Zhang, J. Ma, X. Hu, and Q. Guo, "Effects of Metal Doping on the Catalytic Performance of LaFe-Based Perovskites for CO_2 Hydrogenation to Light Olefins," *Journal of Fuel Chemistry and Technology* 51, no. 1 (2023): 101–110.

120. Y. Wang, S. Lin, M. Li, et al., "Boosting CO_2 Hydrogenation of Fe-Based Monolithic Catalysts via 3D Printing Technology-Induced Heat/Mass-Transfer Enhancements," *Applied Catalysis, B: Environmental* 340 (2024): 123211.

121. O. Elishav, Y. Shener, V. Beilin, et al., "Electrospun Fe–Al–O Nanobelts for Selective CO_2 Hydrogenation to Light Olefins," *ACS Applied Materials & Interfaces* 12, no. 22 (2020): 24855–24867.

122. Z. Zhang, Y. Liu, L. Jia, et al., "Effects of the Reducing Gas Atmosphere on Performance of FeCeNa Catalyst for the Hydrogenation of CO_2 to Olefins," *Chemical Engineering Journal* 428 (2022): 131388.

123. Y. Guo, L. Jia, Z. Zhang, et al., "Revealing the Mechanism of Ce Promoter in Modulating Product Distribution of CO_2 Hydrogenation over Fe-Based Catalysts," *Chemical Engineering Journal* 491 (2024): 151964.

124. H. Raghav, L. N. Siva Kumar Konathala, N. Mishra, et al., "Fe-Decorated Hierarchical Molybdenum Carbide for Direct Conversion of CO_2 Into Ethylene: Tailoring Activity and Stability," *Journal of CO2 Utilization* 50 (2021): 101607.

125. X. Wang, D. Wu, J. Zhang, et al., "Highly Selective Conversion of CO_2 to Light Olefins via Fischer-Tropsch Synthesis Over Stable Layered K–Fe–Ti Catalysts," *Applied Catalysis, A: General* 573 (2019): 32–40.

126. D. Wu, X. Wang, X. Gao, et al., "Preparation of Layered K-Fe-Zn-Ti Catalyst and Its Performance in the Hydrogenation of Carbon Dioxide to Light Olefins," *Journal of Fuel Chemistry and Technology* 47, no. 8 (2019): 949–956.

127. F. Yuan, G. Zhang, M. Wang, et al., "Boosting the Production of Light Olefins From CO_2 Hydrogenation Over Fe–Co Bimetallic Catalysts Derived From Layered Double Hydroxide," *Industrial & Engineering Chemistry Research* 62, no. 21 (2023): 8210–8221.

128. X. Sun, T. Guo, M. An, et al., "The Bifunctional Oxygen Carrier $K/La_yCo_xFe_{1-x}O_3$ for the Production of C_2–C_4 Olefins via CO_2 Hydrogenation," *International Journal of Hydrogen Energy* 51, no. A (2023): 368–381.

129. Y. Zhao, J. Ma, J. Yin, et al., "Alkali Metal Promotion on Fe-Co-Ni Trimetallic Catalysts for CO_2 Hydrogenation to Light Olefins," *Applied Surface Science* 657 (2024): 159783.

130. G. Singh, S. Panda, J. Gahtori, et al., "Comparative Study of Short-Chain Olefins Synthesis via CO_2 Hydrogenation Over Iron-Containing Double Metal Cyanide-Derived Catalysts," *ACS Sustainable Chemistry & Engineering* 11, no. 30 (2023): 11181–11198.

131. D. Mateo, J. L. Cerrillo, S. Durini, and J. Gascon, "Fundamentals and Applications of Photo-Thermal Catalysis," *Chemical Society Reviews* 50, no. 3 (2021): 2173–2210.

132. Y. Li, X. Pei, Z. jun Wang, L. Shi, H. Song, and J. Ye, "Photothermal Catalytic CO_2 Conversion to Value-Added Chemicals: Progress and Prospects," *ACS Sustainable Chemistry & Engineering* 12, no. 47 (2024): 17069–17097.

133. X. Ding, W. Liu, J. Zhao, L. Wang, and Z. Zou, "Photothermal CO_2 Catalysis Toward the Synthesis of Solar Fuel: From Material and Reactor Engineering to Techno-Economic Analysis," *Advanced Materials* 37, no. 2 (2024): 2312093.

134. Q. Xu, Z. Xia, J. Zhang, et al., "Recent Advances in Solar-Driven CO_2 Reduction Over g-C_3N_4-Based Photocatalysts," *Carbon Energy* 5, no. 2 (2023): e205.

135. C. Song, Z. Wang, J. Zhao, et al., "Photothermal Conversion of CO_2 Into Lower Olefins at the Interface of the K-Promoted Ru/Fe_3O_4 Catalyst," *Chem Catalysis* 4, no. 4 (2024): 100960.

136. C. Song, X. Liu, M. Xu, et al., "Photothermal Conversion of CO_2 With Tunable Selectivity Using Fe-Based Catalysts: From Oxide to Carbide," *ACS Catalysis* 10, no. 18 (2020): 10364–10374.

137. C. Song, Z. Wang, Z. Yin, D. Xiao, and D. Ma, "Principles and Applications of Photothermal Catalysis," *Chem Catalysis* 2, no. 1 (2022): 52–83.

138. C. Lv, X. Bai, S. Ning, et al., "Nanostructured Materials for Photothermal Carbon Dioxide Hydrogenation: Regulating Solar Utilization and Catalytic Performance," *ACS Nano* 17, no. 3 (2023): 1725–1738.

139. T. Liu, K. Wang, W. Zhang, et al., "Recent Advances on Dynamic Phase Reconstruction of Fe-Based Catalysts for Catalytic CO_2 Hydrogenation to Long Chain α-Olefins," *Journal of Environmental Chemical Engineering* 12, no. 5 (2024): 113885.

140. C. G. Okoye-Chine, C. O. L. Mbuya, N. C. Shiba, and K. O. Otun, "Effective Catalysts for Hydrogenation of CO_2 Into Lower Olefins: A Review," *Carbon Capture Science & Technology* 13 (2024): 100251.

141. T. M. Karnaukhov, A. A. Vedyagin, S. V. Cherepanova, V. A. Rogov, V. O. Stoyanovskii, and I. V. Mishakov, "Study on Reduction Behavior of Two-Component Fe-Mg-O Oxide System Prepared via a Sol-Gel Technique," *International Journal of Hydrogen Energy* 42, no. 52 (2017): 30543–30549.

142. D. H. Kim, S. W. Han, H. S. Yoon, and Y. D. Kim, "Reverse Water Gas Shift Reaction Catalyzed by Fe Nanoparticles With High Catalytic Activity and Stability," *Journal of Industrial and Engineering Chemistry* 23 (2015): 67–71.

143. Y. A. Daza and J. N. Kuhn, "CO_2 Conversion by Reverse Water Gas Shift Catalysis: Comparison of Catalysts, Mechanisms and Their Consequences for CO_2 Conversion to Liquid Fuels," *RSC Advances* 6, no. 55 (2016): 49675–49691.

144. H. Atashi and F. Rezaeian, "Modelling and Optimization of Fischer–Tropsch Products Through Iron Catalyst in Fixed-Bed Reactor," *International Journal of Hydrogen Energy* 42, no. 23 (2017): 15497–15506.

145. Q. Y. Liu, C. Shang, and Z. P. Liu, "*In Situ* Active Site for CO Activation in Fe-Catalyzed Fischer–Tropsch Synthesis From Machine Learning," *Journal of the American Chemical Society* 143, no. 29 (2021): 11109–11120.

146. P. A. Chernavskii, V. O. Kazak, G. V. Pankina, et al., "Influence of Copper and Potassium on the Structure and Carbidisation of Supported Iron Catalysts for Fischer–Tropsch Synthesis," *Catalysis Science & Technology* 7, no. 11 (2017): 2325–2334.

147. H. Schulz, "Selforganization in Fischer–Tropsch Synthesis With Iron- and Cobalt Catalysts," *Catalysis Today* 228 (2014): 113–122.

148. A. V. Puga, "On the Nature of Active Phases and Sites in CO and CO_2 Hydrogenation Catalysts," *Catalysis Science & Technology* 8, no. 22 (2018): 5681–5707.

149. M. V. Landau, N. Meiri, N. Utsis, R. Vidruk Nehemya, and M. Herskowitz, "Conversion of CO_2, CO, and H_2 in CO_2 Hydrogenation to Fungible Liquid Fuels on Fe-Based Catalysts," *Industrial & Engineering Chemistry Research* 56, no. 45 (2017): 13334–13355.

150. D. Förtsch, K. Pabst, and E. Groß-Hardt, "The Product Distribution in Fischer–Tropsch Synthesis: An Extension of the ASF Model to Describe Common Deviations," *Chemical Engineering Science* 138 (2015): 333–346.